J. Mol. Biol. (1998) **278**, 667–686

JMB

Backbone and Methyl Dynamics of the Regulatory Domain of Troponin C: Anisotropic Rotational Diffusion and Contribution of Conformational Entropy to Calcium Affinity

Stéphane M. Gagné[1], Sakae Tsuda[2], Leo Spyracopoulos[1], Lewis E. Kay[3] and Brian D. Sykes[1]*

[1]*Department of Biochemistry Medical Research Council Group in Protein Structure and Function, University of Alberta, Edmonton, T6G 2H7 Canada*

[2]*Bioscience and Chemistry Division, Hokkaido National Industrial Research Institute Toyohira, Sapporo 062, Japan*

[3]*Protein Engineering Network Center of Excellence and Departments of Medical Genetics, Biochemistry and Chemistry, University of Toronto, Toronto, M5S 1A8 Canada*

**Corresponding author*

The N-terminal domain (residues 1 to 90) of chicken skeletal troponin C (NTnC) regulates muscle contraction upon the binding of a calcium ion to each of its two calcium binding loops. In order to characterize the backbone dynamics of NTnC in the apo state (NTnC-apo), we measured and carefully analyzed ^{15}N NMR relaxation parameters T_1, T_2 and NOE at ^1H NMR frequencies of 500 and 600 MHz. The overall rotational correlation time of NTnC-apo at 29.6°C is 4.86 (±0.15) ns. The experimental data indicate that the rotational diffusion of NTnC-apo is anisotropic with a diffusion anisotropy, $D_{\parallel}/D_{\perp}$, of 1.10. Additionally, the dynamic properties of side-chains having a methyl group were derived from ^2H relaxation data of CH_2D groups of a partially deuterated sample.

Based on the dynamic characteristics of TnC, two different levels of ''fine tuning'' of the calcium affinity are presented. Significantly lower backbone order parameters (S^2), were observed for calcium binding site I relative to site II and the contribution of the bond vector fluctuations to the conformational entropy of sites I and II was calculated. The conformational entropy loss due to calcium binding ($\Delta\Delta S_p$) differs by 1 kcal/mol between sites I and II. This is consistent with the different dissociation constants previously measured for sites I and II of 16 μM and 1.7 μM, respectively.

In addition to the direct role of binding loop dynamics, the side-chain methyl group dynamics play an indirect role through the energetics of the calcium-induced structural change from a closed to an open state. Our results show that the side-chains which will be exposed upon calcium binding have reduced motion in the apo state, suggesting that conformational entropic contributions can be used to offset the free energy cost of exposing hydrophobic groups. It is clear from this work that a complete determination of their dynamic characteristics is necessary in order to fully understand how TnC and other proteins are fine tuned to appropriately carry out their function.

© 1998 Academic Press Limited

Keywords: troponin C; calcium affinity; NMR nitrogen relaxation; NMR deuterium relaxation; conformational entropy

Introduction

Muscle contraction is initiated by the release of Ca^{2+} from the sarcoplasmic reticulum, triggering a cascade of events involving several protein structural changes and altered protein–protein interactions (Farah & Reinach, 1995; Leavis & Gergely, 1984; Ohtsuki *et al.*, 1986; Zot & Potter, 1987). In vertebrate skeletal muscle, the conformational

Presented in part at the ''International Symposium on Protein Condensation – In Honor of Gregorio Weber'' (d. 1997) held in May 1997 in Rio de Janeiro, Brazil.

Abbreviations used: TnC, troponin C; NTnC, N-terminal domain of TnC; NTnC-apo, NTnC in the apo form; NTnC-2Ca, NTnC in the calcium-saturated form; CTnC, C-terminal domain of TnC; TnI, troponin-I; ASA, accessible surface area; NOE, nuclear Overhauser effect.

0022–2836/98/180667–20 $25.00/0/mb981723

© 1998 Academic Press Limited

change in TnC resulting from Ca^{2+} binding is the first event in contraction. TnC is a small acidic protein (18 kDa) consisting of two similar globular domains (NTnC and CTnC), each containing two Ca^{2+} binding sites. NTnC contains calcium binding sites I and II, and carries out the regulatory function. The calcium-induced structural change in NTnC causes new sites of interaction between TnC and TnI (Farah & Reinach, 1995). Hydrophobic residues of NTnC are believed to play a crucial role in the TnC-TnI interactions.

A large amount of structural information on skeletal TnC is now available: X-ray crystal structures of whole TnC where CTnC is in the calcium state and NTnC is in the apo state (Herzberg & James, 1988; Satyshur *et al*., 1988), an early proposed model of the calcium-induced structural change in NTnC (Herzberg *et al*., 1986), NMR solution structures of site IV-site IV homodimer (Kay *et al*., 1991) and site III-site III homodimer (Shaw *et al*., 1992), an NMR solution structure of a TR1C fragment (NTnC minus the first helix) in the apo form (Findlay *et al*., 1994), NMR solution structures of NTnC in both the apo and calcium states (Gagné *et al*., 1995), an NMR solution structure of whole TnC in the calcium state (Slupsky & Sykes, 1995), an NMR solution structure of site III-site IV heterodimer (Shaw & Sykes, 1996), an NMR solution structure of an E41A mutant of NTnC in the calcium form (Gagné *et al*., 1997), and an X-ray crystal structure of NTnC in the calcium form (Strynadka *et al*., 1997). Based on the various structures determined to date, a near complete structural understanding of the mechanism by which TnC regulates muscle contraction has been provided (Gagné *et al*., 1997; Strynadka *et al*., 1997). However, the dynamic properties of TnC have not yet been characterized.

This paper reports a study of the backbone and side-chain dynamics of NTnC in the apo form. Backbone dynamic information is based on ^{15}N relaxation parameter measurements at two fields, 500 and 600 MHz. We determined the overall correlation time and the order parameters of the N–H bond vectors for NTnC-apo. Several motional models were considered in order to appropriately interpret the data. We first analyzed the data using three different isotropic models described by Farrow *et al*. (1994): the simple S^2-τ_e model, the S^2-τ_e-R_{ex} model where the additional term takes into account potential chemical or conformational exchange, and the two-time-scale model. The data were also fitted with a model which included anisotropic rotational diffusion (Tjandra *et al*., 1995). Side-chain methyl group dynamics were obtained from ^2H relaxation measurements of CH_2D groups in a partially deuterated sample (Muhandiram *et al*., 1995).

Based on the dynamic characteristics of TnC, two different levels of ''fine tuning'' of the calcium affinity are presented. Using the relation between entropy and NMR-derived backbone order parameters (Akke *et al*., 1993; Yang & Kay, 1996), the conformational entropy of the calcium-binding loops is obtained, and its contribution to calcium binding affinity is calculated. Additionally, the dynamic properties of the methyl groups provide information on hydrophobic residues which contribute to the energetics of calcium binding and structural change.

Theory

Theoretical expressions for the T_1, T_2 and NOE relaxation parameters of an amide ^{15}N nucleus are well established (Abragam, 1961; Farrow *et al*., 1994). Analysis of the experimental data with the assumption of isotropic rotational diffusion is often done using the ''model-free'' approach where the spectral density function is (Lipari & Szabo, 1982a,b):

$$J(\omega) = S^2\tau_m/(1+\omega^2\tau_m^2) + (1-S^2)\tau/(1+\omega^2\tau^2) \quad (1)$$

where $1/\tau = 1/\tau_m + 1/\tau_e$, S^2 is the order parameter, τ_m is the overall correlation time and τ_e is the effective correlation time representing fast internal motions. For the $S^2 - \tau_e$ model, equation (1) is used as the spectral density in the T_1, T_2 and NOE expressions (equations (4), (5), and (6) of Farrow *et al*. (1994)).

Conformational exchange can be accounted for by incorporating an additional term, R_{ex}, in the T_2 equation:

$$1/T_2 = 1/T_{2(DD)} + 1/T_{2(CSA)} + R_{ex} \quad (2)$$

where $T_{2(DD)}$ and $T_{2(CSA)}$ represent the dipole-dipole and chemical shift anisotropy contributions to the calculated T_2. This is referred in the text as the S^2-τ_e-R_{ex} model analysis, and uses the spectral density function defined in equation (1).

The third model which is considered under the assumption of isotropic tumbling is the two-time-scale model (Clore *et al*., 1990a,b) which accounts for internal motions occurring on two distinct time scales. This extended form of the model-free spectral density is given by the following expression:

$$J(\omega) = S^2\tau_m/(1+\omega^2\tau_m^2) + (S_f^2 - S^2)\tau/(1+\omega^2\tau^2) \quad (3)$$

where $S^2 = S_f^2 S_s^2$ and $1/\tau = 1/\tau_m + 1/\tau_s$. S_f^2 and S_s^2 are the order parameters characterizing the fast and slow internal motions, respectively, and τ_s is the effective correlation time for the slow internal motions. Equation (3) is obtained with the assumption that the term containing the correlation time describing the faster internal motion contributes a negligible amount to the relaxation (Clore *et al*., 1990b).

Determination of the parameters in the spectral density function was done by optimising a χ^2 function given by (Farrow *et al*., 1994):

$$\chi^2 = (T_{1,c} - T_{1,e})^2/\sigma_{T_1}^2 + (T_{2,c} - T_{2,e})^2/\sigma_{T_2}^2 + (NOE_c - NOE_e)^2/\sigma_{NOE}^2 \quad (4)$$

where the subscript c and e represent calculated and experimental parameters, and $\sigma_{T_1,T_2,\mathrm{NOE}}$ are estimates of the error in the experimentally determined parameters. Relaxation analysis assuming isotropic rotational diffusion was performed using programs provided by Farrow *et al*. (1994).

The theory used in the analysis of the relaxation data where anisotropic rotational diffusion is taken into account is as described by Tjandra *et al*. (1995) and will not be repeated here. The error function which is optimized to obtain the anisotropic diffusion parameters is given by:

$$E = \sum_n (T_{1,\mathrm{e}}/T_{2,\mathrm{e}} - T_{1,\mathrm{c}}/T_{2,\mathrm{c}})^2/\sigma^2_{T_1/T_2} \qquad (5)$$

where σ_{T_1/T_2} is the estimated error in the experimental T_1/T_2 ratio, and the summation extends over all residues, N, used in the fit. The calculated T_1/T_2 ratio is given by the ratio of equations (4) and (5) of Farrow *et al*. (1994), and the spectral density function is defined by equation (6) of Tjandra *et al*. (1995). Optimization of equation (5) was performed using in-house programs (S. M. Gagné). Evaluation of the statistical significance of a reduction in the E function when increasing the number of adjustable parameters was performed using the statistical F test (Bevington & Robinson, 1992). The reduced error function is defined as:

$$E_\mathrm{v} = E/(N - m) \qquad (6)$$

where m is the number of variables used in the fitting procedure. A test for the validity of adding x variables is done with the following ratio:

$$F_\mathrm{x} = (E_\mathrm{m} - E_{\mathrm{m+x}})/(xE_{\mathrm{v,m+x}}) \qquad (7)$$

where E_m and $E_{\mathrm{m}+\mathrm{x}}$ are the error functions, E from the fitting which uses m and $m + x$ variables, respectively. A large F_x value justifies the addition of x variables in the fitting. The probability that the observed improvement in the $(m + x)$-parameter fit over the m-parameter fit is obtained by chance is calculated from the normalized integral of the probability density function $P(F_\mathrm{x};\ x;\ N\text{-}m\text{-}x)$. The numerical evaluation of $P(F_\mathrm{x};\ x;\ N\text{-}m\text{-}x)$ was done with the *Mathematica 3.0* package (Wolfram, 1996) using the following *Mathematica* definition:

$$P(F_\mathrm{x};\ x;N\text{-}m\text{-}x) = 1 - \mathrm{CDF}[\mathrm{FRatioDistribution}[x, N\text{-}m\text{-}x], F_\mathrm{x}] \qquad (8)$$

The theory regarding ^{2}H relaxation is described by Muhandiram *et al*. (1995). The relaxation of pure deuterium magnetization is derived in a straightforward manner using the following relations (Muhandram *et al*., 1995):

$$1/T_1^\mathrm{D} = 1/T_1^{\mathrm{I_zC_zD_z}} - 1/T_1^{\mathrm{I_zC_z}} \qquad (9)$$

$$1/T_{1\rho}^\mathrm{D} = 1/T_1^{\mathrm{I_zC_zD_y}} - 1/T_1^{\mathrm{I_zC_z}} \qquad (10)$$

where T_1^D and $T_{1\rho}^\mathrm{D}$ denote pure deuterium relaxation. $T_1^{\mathrm{I_zC_zD_z}}$, $T_1^{\mathrm{I_zC_zD_y}}$ and $T_1^{\mathrm{I_zC_z}}$ are the relaxation parameters which are measured, where I_z, C_z, and D_z denote the z magnetization components of the methyl proton, carbon, and deuteron spins, respectively, and D_y is the y component of deuterium magnetization. It has been established that, under the conditions used here, $1/T_{1\rho}^\mathrm{D} = 1/T_2^\mathrm{D}$ (Muhandiram *et al*., 1995). The spectral density function used in the T_1^D and $T_{1\rho}^\mathrm{D}$ equations (equation (10.2) of Muhandiram *et al*. (1995)) is similar to that for the ^{15}N analysis (equation (1)). However, S^2 represents the order parameter for a methyl group, and describes the spatial motion of the ^{13}C–^{2}H vector on the ns-ps time scale, and is given by $S^2 = S^2_\mathrm{axis}[(3\ \cos^2\theta - 1)/2]^2$. The factor $(3\ \cos^2\theta - 1)/2$ relates to the rapid rotation of the ^{13}C–^{2}H vector about the averaging axis. Assuming tetrahedral geometry ($\theta = 109.5°$), $S^2 = 0.111\ S^2_\mathrm{axis}$. S^2_axis therefore corresponds to the order parameter describing the motion of the averaging axis. Motional parameters were obtained by minimizing the function:

$$\chi^2 = (T_{1,\mathrm{c}} - T_{1,\mathrm{e}})^2/\sigma^2_{T_1} + (T_{1\rho,\mathrm{c}} - T_{1\rho,\mathrm{e}})^2/\sigma^2_{T_{1\rho}} \qquad (11)$$

where the parameters are as described for equation (4).

Results

The primary goal of this work is to relate the dynamic properties of NTnC to its function. However, several technical details need to be presented first in order to establish the validity of the dynamic parameters which are obtained. In a first step, we outline our approach to obtain accurate ^{15}N-T_2 measurements which are not affected by sample heating. Following the acquisition of the experimental ^{15}N relaxation parameters, we determined the overall rotational correlation time under the assumption of isotropic rotational diffusion and using the simple S^2-τ_e spectral density. Under this same assumption, we fitted the ^{15}N relaxation parameters to three different models as described in Introduction and Theory. As will be shown, the ''isotropic'' fits suggest the presence of conformational exchange for a portion of the molecule. As was shown in other studies (Luginbühl *et al*., 1997; Tjandra *et al*., 1995), anisotropic rotational diffusion can easily be mistaken for conformational exchange, and we therefore included anisotropy in the final fitting.

Influence of sample heating on ^{15}N-T_2 measurements

Measurement of ^{15}N-T_2 relaxation data for proteins in solution requires the application of a large number of ^{15}N pulses for various relaxation decay time periods (Farrow *et al*., 1994). Depending on various factors such as decay time duration, power level used, delay between scans, and sample conditions, T_2 experiments are prone to sample heating. In particular, ionic strength, solvent, and γB_2

magnitude can have profound effects on sample heating (Wang & Bax, 1993). Sample heating can lead to inaccurate data in two ways. First, it can directly affect the dynamic properties of the protein which are temperature dependent. Second, since each data point requires a different spin-lock period, the amount of sample heating will vary between data points and adversely affect the observed exponential decay. Care must therefore be taken to avoid or minimize sample heating.

A simple way to reduce heating is to increase the relaxation delay between scans, and we looked at the dependence of the observed T_2 on the relaxation delay. T_2 data were obtained using five different relaxation delays: 1.0, 1.5, 2.0, 2.5 and 3.0 seconds. The precision of each of the T_2 values was estimated as described in Materials and Methods. The accuracy of the different T_2 measurements was estimated by assuming that the data obtained with the longest relaxation delay (3.0 seconds) gave the "correct" T_2 ($T_{2,c}$):

$$\text{accuracy} = (1/N)\sum_n \Delta_{T_2}/T_{2,c} \qquad (12)$$

where Δ_{T_2} is the absolute difference between the T_2 at a given relaxation delay and $T_{2,c}$. The average is over all 74 characterized residues (N). The relation between accuracy of the observed T_2 and the relaxation delay is shown in Figure 1. Although the precision of the various T_2 is nearly constant at ~1%, the accuracy of those values is very poor when using short relaxation delays. For this sample and the experimental conditions described in Materials and Methods, a relaxation delay of 2.5 seconds was necessary to obtain an accuracy of the order of ~1%. The 1.5 second experiment was repeated twice, two weeks apart, and showed that the inaccuracy of 5% was reproducible ("precise") to 1%. These data clearly demonstrate that one can obtain inaccurate T_2, although very precise, if care is not taken to minimize sample heating. In our experience, dielectric heating of the NMR samples due to the electric component of the r.f. field is an insidious problem which is easily avoided by either choosing a long relaxation delay (~ three seconds) or ensuring that the relaxation delay is optimized for the conditions. A relaxation delay of three seconds was used here. Note that a longer relaxation delay also reduces potential problems related to partial water saturation.

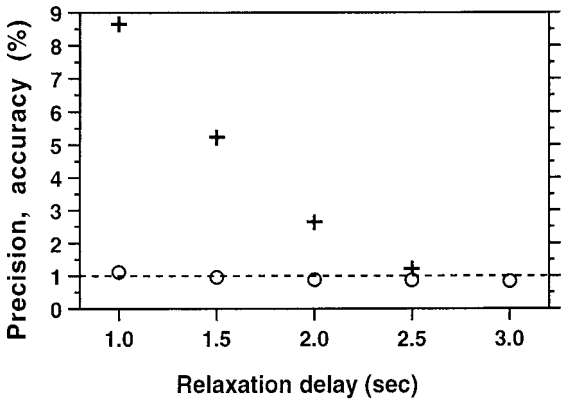

Figure 1. Effect of sample heating and length of the relaxation delay on the precision (○) and accuracy (+) of the measured ^{15}N-T_2. For each delay, the average of all 74 measured T_2 is used. Precision and accuracy were evaluated as described in the text.

^{15}N-T_1, -T_2 and -NOE data

^{15}N relaxation parameters were obtained using 2D ^{1}H−^{15}N correlation NMR spectra. A total of 74 well resolved N−H correlations could be unambiguously characterized and are shown in Figure 2. ^{1}H and ^{15}N assignments were published previously (Gagné *et al.*, 1994). Overlapped resonances were not considered. T_1, T_2 and NOE data were obtained at ^{1}H frequencies of 500 and 600 MHz, and a temperature of 29.6°C. The acquisition of the various data occurred over a period of four months using a single sample. Characteristic fits for the T_1 and T_2 data are shown in Figure 3. The ^{15}N T_1, T_2 and NOE at both frequencies are displayed graphically in Figure 4(a), (b) and (c), respectively.

The T_1^{500}, T_2^{500} and T_2^{600} parameters were measured once, and the corresponding average errors estimated from the fits were 0.8%, 0.8% and 0.9%, respectively. The T_1^{600} experiment was repeated twice using slightly different parameters, and the average is reported. The two T_1^{600} data sets indicated an average error of 0.9%, when estimated from the fit. The average difference between the two T_1^{600} data sets and their average was 0.7%. On the basis of the various errors estimated here, the minimum error on the T_1 and T_2 parameters was set to 1%. For residues where the estimated error from the fitting was larger than 1%, this larger value was used. Usually, the error associated with the NOE parameters is larger than that for the T_1 and T_2, primarily due to the lower signal-to-noise of the NOE experiment. The NOE^{500} and NOE^{600} experiments were repeated three and four times, respectively. Estimates of the error based on noise rms were 1.5% and 1.0% for NOE^{500} and NOE^{600}, respectively. Estimates of the error based on the standard deviation between the repeated experiments was 2.2% and 1.3% for the NOE^{500} and NOE^{600}, respectively. The average errors estimated from the standard deviations were used as minimum errors for the NOE data.

Typically, residues with an NOE$^{500} > 0.60$ or NOE$^{600} > 0.65$ satisfy the condition $\tau_e \ll \omega_H^{-1}$ and, for an isotropically tumbling protein, very fast internal motions on a time scale τ_e do not affect the T_1/T_2 ratio. In NTnC-apo, 60 residues have an NOE$^{500} > 0.60$, and 63 residues have an NOE$^{600} > 0.65$. For the 60 residues with NOE$^{500} > 0.60$, the average T_1^{500}, T_1^{600}, T_2^{500}, T_2^{600},

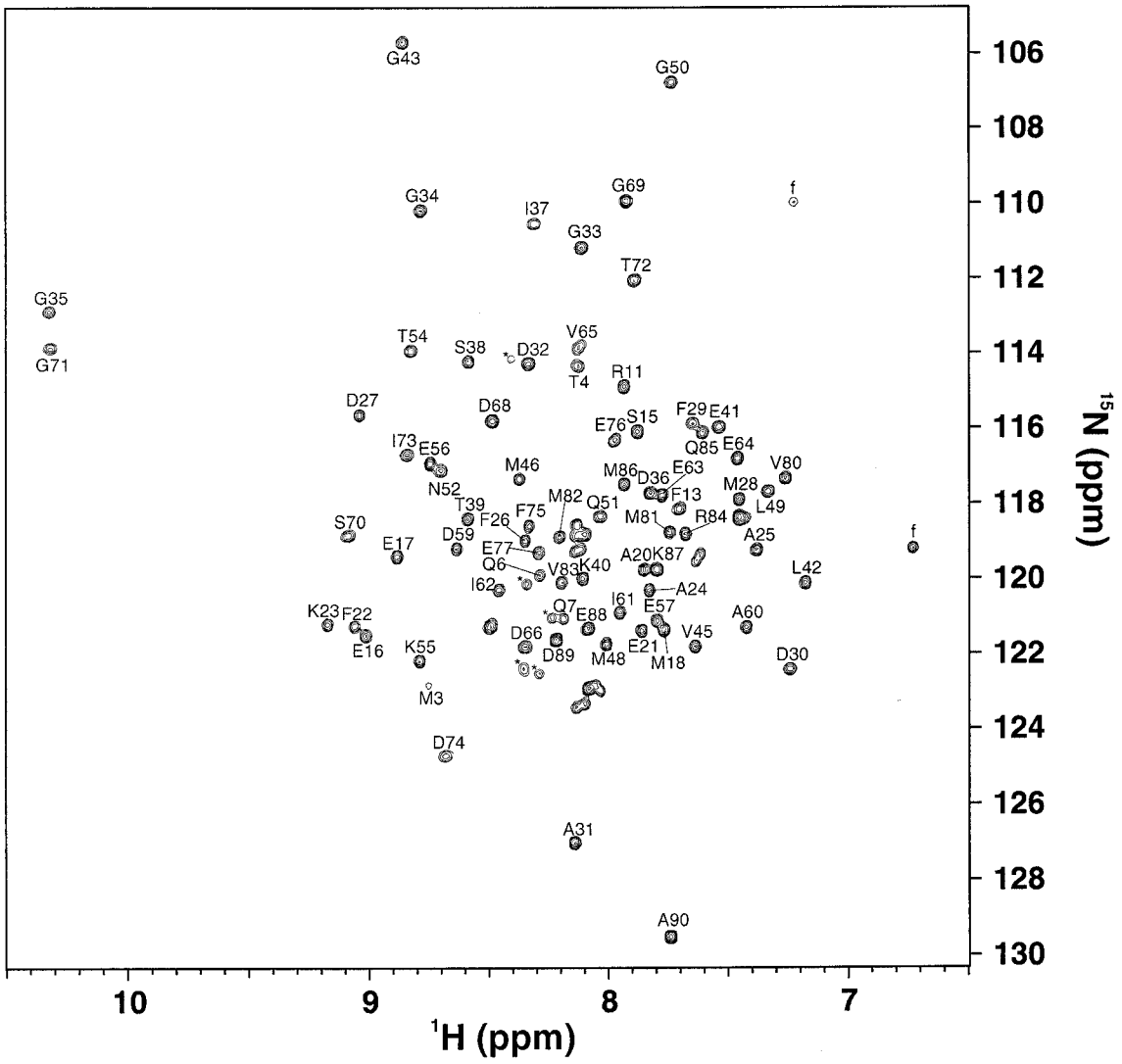

Figure 2. 2D ^{1}H-^{15}N HSQC correlation spectra of NTnC-apo. The 74 residues for which relaxation data were characterized are labeled with their residue name and number. Folded peaks from upfield arginine side-chains are labeled (f), and impurity peaks labeled (*).

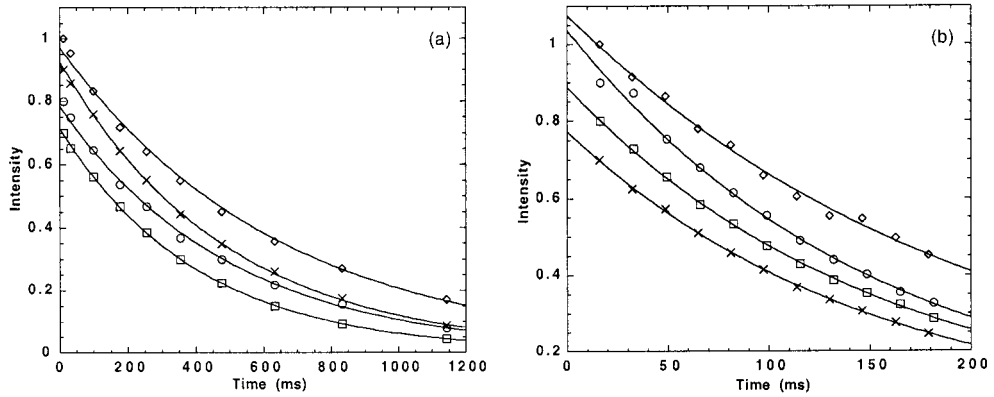

Figure 3. Representative ^{15}N-T_1 (a) and ^{15}N-T_2 (b) relaxation decays obtained in the present study. The following typical decays with errors of approximately 1% are shown: T_1^{500} (Met28, 410.2 (±4.1) ms, □), T_1^{600} (Glu76, 496.5 (±5.0) ms, ×), T_2^{500} (Val65, 160.2 (±1.6) ms, □), T_2^{600} (Ile37, 156.0 (±1.6) ms, ×). Additionally, the worst fit for each experiments is shown: T_1^{500} (Thr4, 477.1 (±10.8) ms, ○), T_1^{600} (Asn52, 630.5 (±15.3) ms, ◇), T_2^{500} (Gly43, 157.4 (±4.2) ms, ○), T_2^{600} (Thr4, 204.8 (±5.0) ms, ◇).

NOE^{500}, NOE^{600} are 413 (±22) ms, 508 (±27) ms, 154 (±11) ms, 151 (±11) ms, 0.68 (±0.04) and 0.76 (±0.04), respectively.

As expected, T_1^{600} is larger than T_1^{500}, but the pattern of the T_1 data is similar at both fields (Figure 4(a)). This is emphasized in the

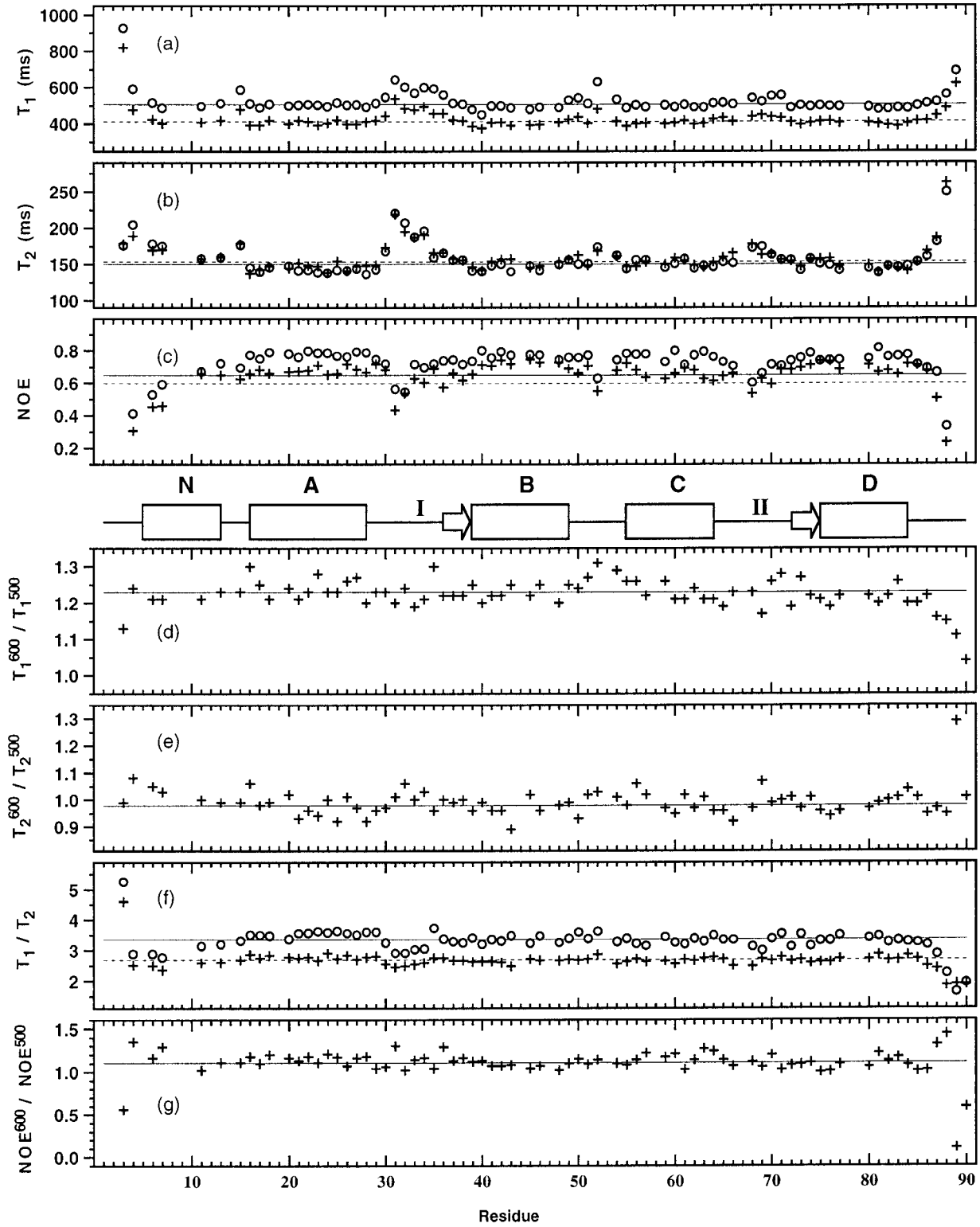

Figure 4. Sequential plots of the measured ^{15}N-T_1 (a), ^{15}N-T_2 (b), and ^{15}N-NOE (c) at 500 (+) and 600 (○) MHz. Also shown are the sequential plots of the T_1^{600}/T_1^{500} ratio (d), T_2^{600}/T_2^{500} ratio (e), T_1/T_2 ratio (f) at 500 (+) and 600 (○) MHz, and NOE^{600}/NOE^{500} ratio (g). The lines in all plots except (c) indicate the average values for residues with $NOE^{500} > 0.60$ at 500 (- - - -) and 600 (——) MHz. In plot (c), the lines indicate NOE = 0.60 (- - - -) and NOE = 0.65 (——). The secondary structure elements of NTnC-apo are shown between plots (c) and (d), where the helices are labeled N, A, B, C, and D, and the two calcium binding loops are labeled I and II.

T_1^{600}/T_1^{500} ratio shown in Figure 4(d). With the exception of the N and C-terminal residues, the T_1^{600}/T_1^{500} ratio is relatively constant with an average ratio of 1.23 (±0.03) for the 60 residues having an $NOE^{500} > 0.60$. Figure 4(b) and (e) clearly indicate that T_2^{500} and T_2^{600} are nearly equivalent for the majority of residues. The T_2^{600}/T_2^{500} ratio is slightly smaller than 1 with an average ratio of 0.98 (±0.04) for residues with $NOE^{500} > 0.60$. It should be noted that the contribution from dipole-dipole relaxation to T_2 ($T_{2(DD)}$) is expected to be, for all purposes, identical at both fields. On the other hand, the contribution from chemical shift anisotropy relaxation to T_2 ($T_{2(CSA)}$) is proportional to $1/\omega_N^2$. Thus, the difference between the $T_{2(CSA)}$ at the two fields predicts $T_2^{500} > T_2^{600}$. The T_1/T_2 ratio, which can be used to determine the overall correlation time (Farrow *et al*., 1994), is plotted in Figure 4(f) for both fields. The average T_1^{500}/T_2^{500} and T_1^{600}/T_2^{600} ratios are 2.69 (±0.09) and 3.37 (±0.17), respectively. Theory predicts that $NOE^{600} > NOE^{500}$, as is observed in the data presented here (Figure 4(c) and (g)). The average NOE^{600}/NOE^{500} ratio is 1.11 (±0.06) for residues with $NOE^{500} > 0.60$.

Determination of the overall correlation time (τ_m)

Although it is possible to simultaneously fit the data at both fields to characterize the molecular motion of NTnC-apo, we chose to treat the 500 and 600 MHz data separately. The advantage of this approach is that each parameter (τ_m, S^2, τ_e, R_{ex}, ...) is independently determined twice.

The first step in the dynamics analysis is the determination of the overall correlation time (τ_m) of NTnC-apo. We first used an approach similar to the one presented by Farrow *et al*. (1994) which assumes that the overall tumbling motion of NTnC-apo is isotropic. The validity of this assumption can be verified by examining the known structure of NTnC-apo. The relative lengths of the principal axes of the inertia tensor of NTnC-apo were determined to be 1.00:0.91:0.85, calculated using residues 2 to 90 of the X-ray structure (Herzberg & James, 1988). The assumption of isotropic motion is therefore, to a first approximation, valid.

A grid search in which the order parameter (S^2) and the effective correlation time (τ_e) were optimized in equation (4) was used to determine a τ_m for each residue. The $S^2 - \tau_e$ spectral density model (equation (1)) was used for the calculated values in equation (4). Table 1 reports the average optimum τ_m and the global optimum τ_m for residues with $NOE^{500} > 0.60$ or $NOE^{600} > 0.65$. Although the estimated error from the standard deviation of the average τ_m is 0.15 (500 MHz) and 0.18 ns (600 MHz), the consistency between the 500 and 600 data could suggest that τ_m is accurate to ~0.03 ns. However, even if the experimental data used to obtain the τ_m at both fields are independent, there are several possible common sources of error, such as the choice of the spectral density model, the assumption of isotropic motion, the value of r_{NH} used (1.02 Å) and the value of $\sigma_\parallel - \sigma_\perp$ used (−160 ppm). We therefore do not believe the τ_m reported here to be accurate to ~0.03 ns, although it appears that we can determine it to that precision. Of course, several independent measurements would be necessary to estimate the real precision of the τ_m reported here. Despite this, the standard deviation of the averages can be used for a conservative estimate of the precision. Thus, the overall correlation time of NTnC-apo is 4.86 (±0.15) ns at 29.6°C.

Table 1. Summary of overall correlation time (τ_m) determination with the isotropic model

Data set	$\langle\tau_m\rangle$[a]	Global τ_m[b]	$\langle\chi^2\rangle$[c]
500 MHz	4.87 ± 0.15 (60)	4.88	1.66
600 MHz	4.84 ± 0.18 (63)	4.84	3.77

[a] Average τ_m obtained from individual fit for residues with $NOE^{500} > 0.60$ or $NOE^{600} > 0.65$. Number of residues used is shown in parentheses.
[b] τ_m which best fit all residues.
[c] Average χ^2 for the optimum τ_m. $\langle\chi^2\rangle = (1/kN)\ \Sigma_N\chi^2$, where χ^2 is as defined in equation (4), N is the number of residues and k is the number of measured variables. In the present case, k is equal to 3, and N is equal to 60 and 63 for the 500 and 600 MHz data, respectively.

Backbone analysis under the assumption of isotropic rotational diffusion

Relaxation data are most commonly interpreted with the model-free formalism for internal motion (Lipari & Szabo, 1982a,b), where the spectral density is represented as a function of the overall correlation time τ_m, the order parameter S^2, and the effective correlation time for internal motions τ_e (equation (1)). Isotropic motion is assumed. The results from this analysis were obtained during the evaluation of τ_m, and are plotted in Figure 5(a) and (b) for both fields. The order parameters at 500 and 600 MHz have an rms of 0.02 over all residues except Asp89. The average S^2 for residues with $NOE^{500} > 0.60$ is 0.85 (±0.05) and 0.84 (±0.05) for the 500 and 600 data, respectively. Not surprisingly, the N and C-terminal regions are flexible. Additionally, the calcium binding loops have lower order parameters, with site I being more flexible than site II. The Gly-Gly-Gly sequence which is found in site I, but not in site II, likely contributes to this greater flexibility. The B-C linker, which is exposed in the NTnC-apo structure, also has lower order parameters. Finally, helix-N also appears to be somewhat more flexible than the other helices. Unfortunately, there are several amides from helix-N which could not be characterized due to partial overlap.

Although the data presented are consistent between the two data sets, the τ_e^{500} and τ_e^{600} are systematically different with average values of 62 and

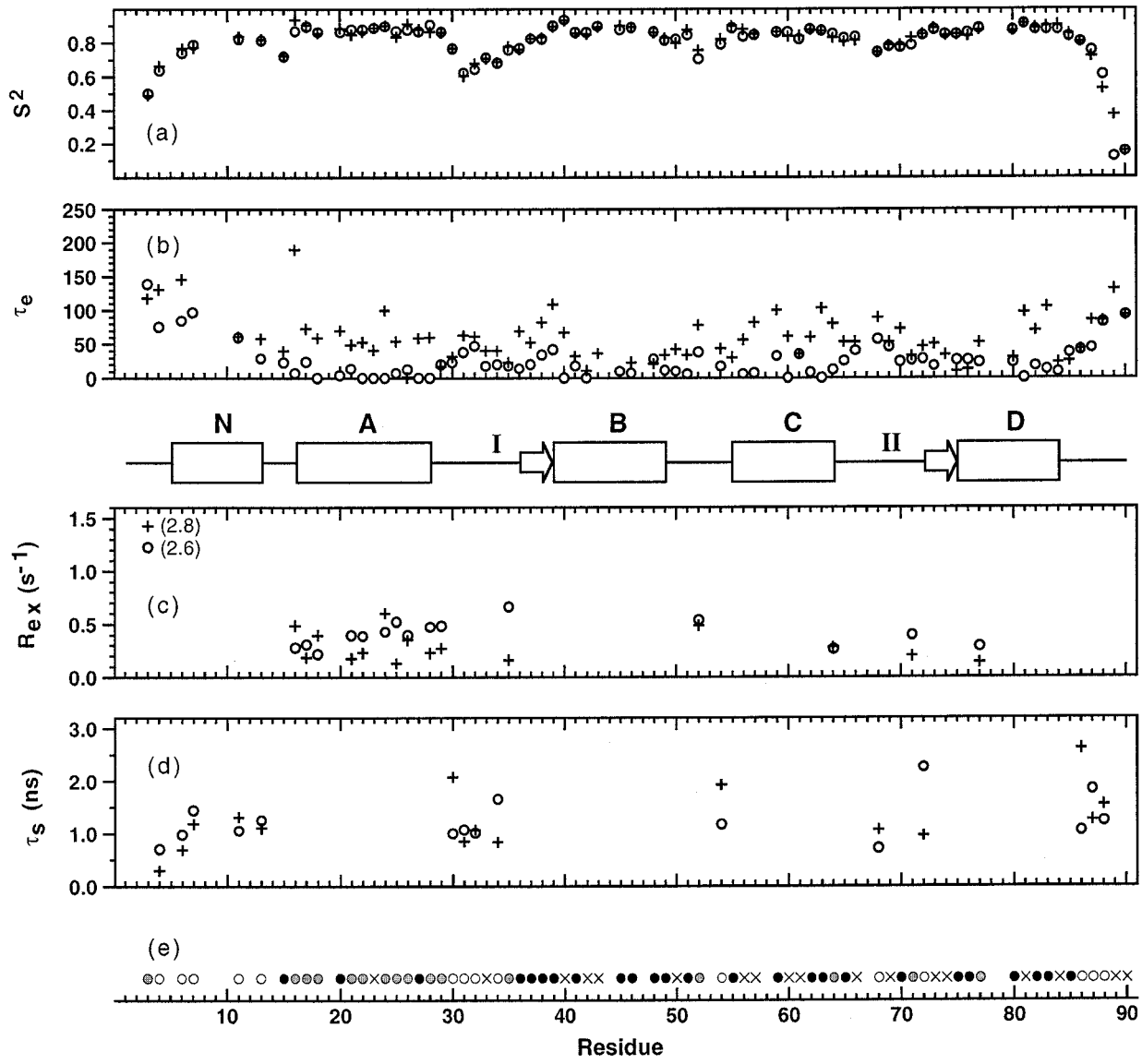

Figure 5. Sequential plots summarizing the various fits made under the assumption of isotropic tumbling. Results for all residues from the S^2-τ_e spectral density are in (a) and (b) for both the 500 (+) and 600 (○) MHz data. Residues which require inclusion of an R_{ex} term in the T_2 or use of the two-time-scale spectral density are shown in (c) and (d), respectively. The optimum R_{ex} value is shown in (c), and the optimum slower effective correlation time (τ_s) is shown in (d). The model which was selected for each residue is illustrated in (e), where S^2-τ_e is indicated by (●), S^2-τ_e-R_{ex} by (◍), two-time-scale by (○), not well-fit with any models by (×), and not characterized by ( ). Secondary structure elements illustrated as in Figure 4.

33 ps, respectively. While interpretation of τ_e values is often not attempted due to the large uncertainty associated with this parameter, we tried to find an explanation for this difference. The discrepancy is due to a larger than expected NOE^{600}/NOE^{500} ratio. Using the spectral density described in equation (1), and values of 4.86 ns and 0.85 for τ_m and S^2, respectively, a NOE^{600}/NOE^{500} ratio in the 1.05 to 1.02 range is predicted, corresponding to τ_e ranging from 0 to 100 ps. As noted above, the observed ratio is actually 1.11 (±0.06). There is evidently at least one NOE data set which contains a systematic error.

For several residues, the S^2-τ_e spectral density did not provide a good fit, i.e. the relaxation parameters (T_1, T_2 and NOE) were not fit within 95% confidence limits. For those residues which did not fit well with the S^2-τ_e model, two alternative isotropic models were tested: one which included an exchange term in the T_2 equation, and another which corresponds to a two-time-scale model (Clore *et al.*, 1990a,b).

The relaxation parameters were therefore fitted with a S^2-τ_e-R_{ex} model (equations (1) and (2)). As before, the 500 and 600 MHz data were treated separately. The inclusion of an R_{ex} parameter in the analysis of a residue was considered valid if it satisfied the following two conditions. First, all three relaxation parameters must be fit within 95% confidence limits. Second, the fitted R_{ex} must be

significant, i.e. its value must be greater than its associated error. Further, these two conditions must also be satisfied for both the 500 and 600 MHz data; therefore the R_{ex} term is considered appropriate only if data at both fields independently validate its use. The 16 residues which fulfilled these requirements are shown with their R_{ex} values in Figure 5(c). With the exception of Met3, the other 15 residues were fit with an average R_{ex}^{500} and R_{ex}^{600} of 0.26 (±0.14) s^{-1} and 0.39 (±0.12) s^{-1}, respectively. Interestingly, 10 of the 16 residues which require a R_{ex} parameter are located in helix-A. The other residues are somewhat scattered and not located within spatial proximity in the structure. As was shown in other studies, conformational exchange can sometimes be a misinterpretation of the experimental data when anisotropic rotational diffusion is present. The presence of conformational exchange needs to be validated and one can look at the $R_{ex}^{600}/R_{ex}^{500}$ ratio which should theoretically be equal to $600^2/500^2$, or 1.44. The ratio for helix-A is scattered with an average of 1.84 (±1.28). One third of helix-A residues which are better fit with an R_{ex} term actually have an R_{ex}^{500} greater than R_{ex}^{600} ($R_{ex}^{600}/R_{ex}^{500}$ of 0.57 (±0.40), 0.55 (±0.28), 0.72 (±0.22) for residues 16, 18, and 24, respectively). This suggests that conformational exchange is not an appropriate interpretation of the experimental data for helix-A.

The third isotropic fit we have used is the two-time-scale approach proposed by Clore *et al.* (1990a,b) and described by equation (3). Selection of this model for a residue was as described above for the S^2-τ_e-R_{ex} model. A total of 15 residues localized in three distinct regions were best fit with the two-time-scale model, as illustrated in Figure 5(d). The first two regions are the calcium binding loops (residues 30, 31, 32, 34, 68 and 72) and the C-terminal end (residues 86, 87, 88). This is not surprising, since loops and terminal ends are likely to have additional motion on the nanosecond time scale. The third region which is best fit with this model is helix-N (residues 4, 6, 7, 11, and 13). It should be noted that there is a gradient in the correlation time for the slower internal motion: τ_s gradually increases from the free N-terminal end to C-terminal end of helix-N. This strongly suggests that helix-N is partially unstructured.

Figure 5(e) summarizes the results from the different fits which were made under the assumption of isotropic rotational diffusion. Of the 74 residues for which relaxation data were analyzed, 25 are best fit with the S^2-τ_e model, 16 required an exchange term (R_{ex}), and 15 needed the two-time-scale model. 18 residues did not give a satisfactory fit by the criteria listed above.

Rotational diffusion anisotropy

As pointed out by Tjandra *et al.* (1995), the presence of rotational diffusion anisotropy could, under certain circumstances, be misidentified as conformational exchange. That a whole helix requires an R_{ex} term in order to have a good fit is actually compatible with diffusion anisotropy. Conformational exchange leads to a reduction of the T_2 and does not affect the T_1. Helix-A shows the shortest average T_2, but also has a slightly longer average T_1 value compared to the other three well structured helices (B, C and D-helices). In other words, the T_1/T_2 ratio of helix-A is significantly larger, suggesting rotational diffusion anisotropy. As noted previously, the principal components of the inertia tensor, with a relative ratio of 1.00:0.91:0.85, suggest very little anisotropy. However, a recent study of the rotational diffusion anisotropy of ubiquitin has shown that even slight anisotropic diffusion can be reflected in the relaxation data (Tjandra *et al.*, 1995). A study from Luginbühl *et al.* (1997) also showed that in some cases the two-time-scale model can provide a misleading view of the internal motions when anisotropic global rotation is present. We therefore considered the anisotropy of NTnC-apo in our analysis in a manner similar to Tjandra *et al.* (1995).

Residues with $NOE^{500} > 0.60$ or $NOE^{600} > 0.65$ which did not indicate conformational exchange (Tjandra *et al.*, 1995) were selected to explore the anisotropy of NTnC-apo. The following condition was used to identify conformational exchange:

$$(\langle T_2\rangle - T_{2,n})/\langle T_2\rangle - (\langle T_1\rangle - T_{1,n})/\langle T_1\rangle > 1.5\sigma \quad (13)$$

where $T_{2,n}$ is the T_2 of residue n, and $\langle T_2\rangle$ is the average T_2. σ is equal to 0.035 (500 data) and 0.054 (600 data) and is the standard deviation of $(\langle T_2\rangle - T_{2,n})/\langle T_2\rangle - (\langle T_1\rangle - T_{1,n})/\langle T_1\rangle$. Note that residues from helix-A are not excluded by this condition, since these residues have opposite fractional changes in T_1 and T_2 (Tjandra *et al.*, 1996). Also, only residues which were located in helices and β-sheets were considered, since loop residues are usually less well defined, and a single H-N vector orientation might not be representative. Using these conditions, 41 and 47 residues were selected from the 500 and 600 MHz data, respectively, to determine if rotational anisotropy was present in NTnC-apo. The data were fit to three models for the diffusion tensor (Tjandra *et al.*, 1995): isotropic, axially symmetric and fully anisotropic. The parameters which characterize the anisotropic models are as defined by Tjandra *et al.* (1995): the diffusion anisotropy is given by $D_\parallel/D_\perp$, which is equivalent to $2D_z/(D_x + D_y)$, the orientation of D_z is a function of θ and ϕ (spherical polar coordinates), and the orientations of D_x and D_y are defined by a third angle, ψ. D_x, D_y and D_z represent the magnitudes of the principal components of the diffusion tensor. The correlation time $\tau_{m,eff}$ is calculated from $(6D)^{-1}$ where $D = (D_x + D_y + D_z)/3$. Coordinates from the crystal structure of NTnC-apo were used for the analysis (PDB accession code 5TNC).

We have characterized the diffusion anisotropy of NTnC-apo and the results are shown in Table 2. As evident by the decrease in the error function,

Table 2. Experimental diffusion parameters for NTnC-apo

Model		$\tau_{m,eff}$[a] (ns)	$D_{\parallel}/D_{\perp}$[b]	D_x/D_y	θ[c] (deg.)	ϕ[c] (deg.)	ψ[c] (deg.)	E[d]	E_v[e]	F_x[f]
Isotropic	500	4.82	1	1				102	2.5	
	600	4.83	1	1				379	8.2	
	Avg.	4.82	1	1				241	5.4	
Ax. symm.	500	4.82	1.07	1	5	−171		74	2.0	4.6
	600	4.81	1.13	1	12	−66		205	4.8	12.2
	Avg.	4.82	1.10	1	8	−118		140	3.4	8.4
Asymm.	500	4.80	1.10	1.07	8	−152	73	68	1.9	1.7
	600	4.83	1.13	1.07	13	−13	65	188	4.6	1.9
	Avg.	4.81	1.11	1.07	11	−83	69	128	3.3	1.8

[a] Effective correlation time, defined as $(6D)^{-1}$.
[b] Defined as $2D_z/(D_x + D_y)$.
[c] Euler angles describing the orientation of the diffusion tensor in the PDB coordinate frame (accession code 5TNC).
[d] Error function (equation (5)).
[e] Reduced error function (equation (6)).
[f] A test for the validity of adding x variables to the fitting procedure (equation (7)).

the fit is better with an axially symmetric diffusion tensor than with an isotropic diffusion tensor. As presented in Theory, the significance of the decrease in the error function was evaluated using the statistical *F*-test (Bevington & Robinson, 1992). The probability that the improvement observed with the inclusion of additional parameters occurred by chance is obtained from $P(F_x; x; N\text{-}m\text{-}x)$ (see Theory). For the axially symmetric model, these probabilities are 8×10^{-3} and 8×10^{-6} for the 500 and 600 MHz data, respectively, therefore justifying the inclusion of the additional terms in the fit, relative to the isotropic model. The fully asymmetric model provides a more modest improvement, relative to the axially symmetric model, as shown by the smaller average F_x. The corresponding $P(F_x; x; N\text{-}m\text{-}x)$ are 0.19 and 0.17 for the 500 and 600 MHz data, respectively. The D_x/D_y ratio and ψ obtained for the fully asymmetric model are therefore not considered statistically significant, and the axially symmetric diffusion tensor model is chosen to best represent the motion of NTnC-apo. Note that for the axially symmetric model we have considered both the oblate ($D_{\parallel} < D_{\perp}$) and the prolate model ($D_{\parallel} > D_{\perp}$), and

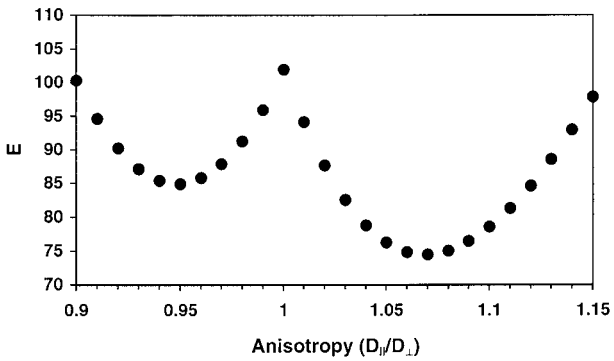

Figure 6. Comparison between oblate ($D_{\parallel} < D_{\perp}$) and prolate ($D_{\parallel} > D_{\perp}$) for the axially symmetric anisotropic fitting of the 500 MHz data. For each point, the anisotropy and the correlation time (4.82 ns) were kept constant, while the orientation of $D_{\parallel}$ was optimized.

Figure 6 shows that NTnC-apo is best represented by a prolate model.

The $\tau_{m,eff}$, $D_{\parallel}/D_{\perp}$ and θ obtained from the axially symmetric model are consistent for the 500 and 600 MHz data, whereas the ϕ angle is less well determined. Note that it is not surprising that the ϕ angle is poorly defined, given that θ is near 0°. The $\tau_{m,eff}$ obtained here is, for all purpose, identical to the one obtained above using the isotropic diffusion model. The small difference in the isotropic τ_m in Tables 1 and 2 is due to the different approach and residues used in the evaluations. The average $D_{\parallel}/D_{\perp}$ ratio of 1.10 is small, as expected from the near symmetric inertia tensor of NTnC-apo. In fact, it is smaller than the $D_{\parallel}/D_{\perp}$ ratio of 1.17 obtained for ubiquitin (Tjandra *et al.*, 1995).

Using the θ and ϕ angles determined above, we calculated the orientation of the various helices with respect to the unique axis of the diffusion tensor. Table 3 summarizes the relaxation parameters and orientations of the helices of NTnC-apo. As expected from the consistency of the experimental data, both the 500 and 600 data indicate a similar orientation for the helices. Based on helix orientation, and the average backbone amide H-N vector orientation, helices N, B, C and D are nearly perpendicular to the $D_{\parallel}$ axis of the diffusion tensor. Helix A, on the other hand, is nearly parallel to $D_{\parallel}$. This is represented graphically in Figure 7. The peculiar orientation of helix A relative to the diffusion tensor can therefore explain the larger T_1/T_2 ratio observed for this helix. The anisotropy of the molecular tumbling, although small, provides an explanation for the relaxation parameters of helix A.

The order parameters were evaluated by taking into account the rotational anisotropic diffusion of NTnC-apo. Using a spectral density function which takes into account rotational anisotropic diffusion (equation (6) of Tjandra *et al.*, 1995), we evaluated S^2 and τ_e in the same manner as for the isotropic S^2-τ_e model. The average anisotropic tumbling parameters obtained for the axially symmetric model were used for the fit (Table 2).

Table 3. T_1/T_2 ratio of the five helices of NTnC-apo and orientation of N-H vectors relative to the axially symmetric diffusion tensor

Parameter	Helix[a] N	A	B	C	D
T_1^{500}/T_2^{500}	2.51 ± 0.11	2.78 ± 0.07	2.64 ± 0.09	2.67 ± 0.07	2.72 ± 0.09
T_1^{600}/T_2^{500}	3.00 ± 0.21	3.54 ± 0.07	3.36 ± 0.10	3.32 ± 0.12	3.36 ± 0.08
Angle (°)[b]	75 ± 14	19 ± 9	63 ± 11	79 ± 8	67 ± 11

[a] Helices defined using the following residue ranges: N (5 to 13), A (16 to 28), B (39 to 48), C (55 to 64), and D (75 to 85).
[b] Average angle between the N–H vectors of the helix and the principal axis of the diffusion tensor ($D_\parallel$).

Comparison of the results from the S^2-τ_e isotropic and anisotropic analysis does not show any significant differences. The rms difference between isotropic and anisotropic fits is 0.003 for S^2, and 5 ps for τ_e. These differences are well within experimental error and indicate that inclusion of anisotropy is not necessary for the evaluation of the backbone order parameters for NTnC-apo, a result which is consistent with other studies (Tjandra *et al*., 1995). The inclusion of anisotropy is however necessary for the selection of the appropriate model. Of the ten residues from helix-A which required the inclusion of an exchange term under assumption of isotropic tumbling, eight are well fit using the S^2-τ_e model when anisotropic tumbling is taken into account. For those eight residues, the average χ^2 for the S^2-τ_e model is reduced from 9.4 (±3.9) to 3.3 (±2.6) upon inclusion of anisotropic tumbling in the analysis.

Methyl group dynamics

We have also studied the side-chain dynamics of NTnC-apo using the approach of Muhandiram *et al.* (1995) where the T_1^D and $T_{1\rho}^D$ relaxation times are measured in uniformly ^{13}C-labeled and fractionally ^2H-labeled samples. The quality of the data can be appreciated from the correlation spectra and decay curves which are shown in Figure 9 and 10 of Spyracopoulos *et al*. (1998). Relaxation data were obtained for 44 methyl groups of NTnC-apo. The T_1^D and $T_{1\rho}^D$ data are represented graphically in Figure 8(a) and (b), and the derived S^2_{axis} are shown in Figure 8(c). The data are presented on the basis of methyl group type in order to compare the motion of a particular methyl with methyl groups of the same nature.

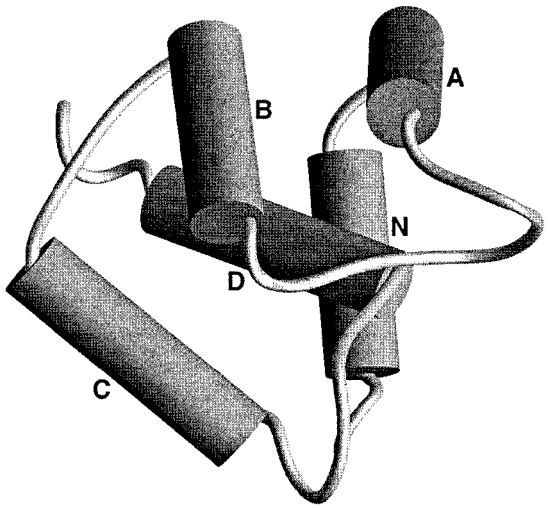

Figure 7. Representation of the structure of NTnC-apo (Herzberg & James, 1988) relative to the axially symmetric diffusion tensor. Helices are shown as cylinders. In this orientation $D_\parallel$ is perpendicular to the page, clearly showing that it is nearly parallel to helix-A and more perpendicular to the other four helices. This Figure was made with the program Ribbons (Carson, 1987).

The backbone order parameters are also shown in Figure 8(c) to indicate the motion of a methyl group relative to its backbone motion. For alanine residues, the methyl order parameters are similar to those of the backbone since the C^α–C^β bond is part of the backbone structure. For all other residue types, the S^2_{axis} of methyl groups is significantly smaller than the S^2 of the H-N vector because of additional degrees of freedom. The difference between the S^2 of the backbone amide and the S^2_{axis} of the methyl group is primarily a function, though not exclusively, of flexibility of the dihedral angles between the methyl group and the backbone. For example, the large difference for Thr4 indicates a poorly defined χ_1 dihedral angle, whereas Thr54 appears to have a well-defined χ_1. Using this relation, the isoleucine$^{\gamma 2}$ and valine data indicate that Ile37, Ile62, Val80 and Val83 have relatively well-defined χ_1 angles compared to Ile73, Val45 and Val65. The larger difference observed for Ile62$^{\delta 1}$ compared to Ile62$^{\gamma 2}$ indicates that although the χ_1 of this residue shows little variability, the χ_2 angle is less restricted. All but one of the methionine residues have a very disordered methyl group. Met82 is the only restricted methionine methyl group.

Figure 8(c) also shows the ''normal'' distribution of S^2_{axis} for each methyl type. The distribution was calculated from all S^2_{axis} obtained using the ^2H relaxation approach and published to date. As expected, the distribution of S^2_{axis} for alanine residues is similar to the S^2 of H–N vectors, with an average of 0.83 (±0.11). The relative position of the average of the other methyl types is in agreement with the nature of the particular side-chain. With the exception of terminal residues Ala1, Met3, Thr4 and Ala90, the other methyl groups which significantly fall outside of the expected distribution are

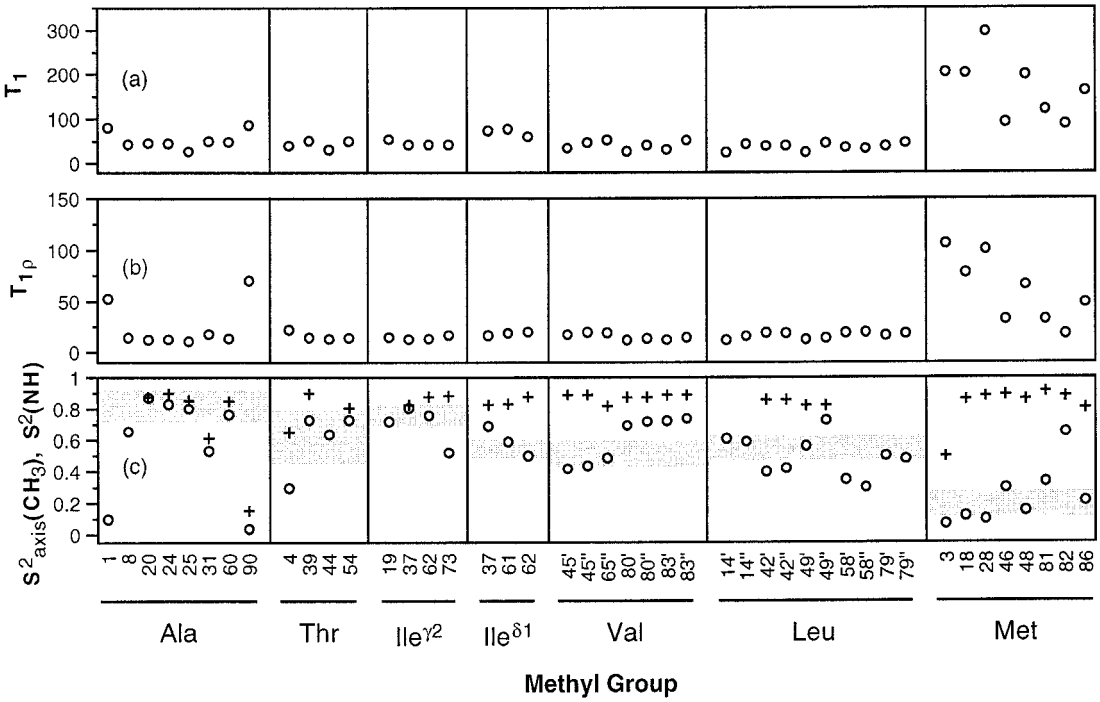

Figure 8. Plots of the measured methyl CH_2D ^2H-T_1 (a) and ^2H-$T_{1\rho}$ (b) at 600 MHz on a per-residue type basis. The derived order parameter of the averaging axis of the methyl groups (○) are shown in (c) along with the corresponding backbone ^{15}N order parameter (+). The shaded areas in (c) represent the average ±one standard deviation for each residue type, obtained from this work and other published data (Kay *et al.*, 1996).

of interest. Therefore Ala8, Ala31, Ile73$^{\gamma 2}$ and Leu58 can be looked at as having larger motion than usually observed. Using the same analogy, the S^2_{axis} of Ile37$^{\delta 1}$, Val80, Val83, and Met82 indicate that those residues have reduced motion, most likely due to tight packing of the methyl group on other hydrophobic residues.

When comparing the solvent ASA of the side-chains, one finds that there is not always a direct correlation between these two parameters as pointed out previously (Kay *et al.*, 1996), although generally more exposed residues will have lower order parameters. Of the six non-terminal methionine residues in NTnC-apo, three are exposed and three are buried. Met18, Met28, and Met48 are exposed in the NMR structure (Gagné *et al.*, 1995) with side-chain solvent ASA of 94 (±11) Å^2, 129 (±16) Å^2, and 124 (±17) Å^2, respectively (the corresponding values in the crystal structure (Herzberg & James, 1988) are 70 Å^2, 137 Å^2, and 85 Å^2). Met46, Met81, and Met82 are more buried in the NMR structure with solvent ASA of 11 (±9) Å^2, 20 (±9) Å^2, and 27 (±11) Å^2, respectively (the corresponding values in the crystal structure are 0 Å^2, 4 Å^2, and 0 Å^2). Although the three exposed methionine residues have lower order parameters than the three buried ones (Figure 8(c)), one cannot quantitatively relate solvent ASA to order parameters when comparing the three buried methionine residues. For example, Met46, Met81, and Met82 have similar solvent ASA, but the order parameter of Met82 is significantly larger than the other two (Figure 8(c)). Therefore one should be cautious when attempting to correlate solvent ASA and flexibility.

Discussion

The quality of the relaxation data presented here is high, as highlighted by the consistency between the 500 and 600 MHz data sets. The analysis was first carried out with the assumption of isotropic tumbling, but the presence of slight anisotropy leads to misinterpretation of the experimental data. Anisotropic tumbling was therefore included in the analysis. The main goal of this study was to relate relaxation parameters of both backbone amides and side-chain methyls to the structure and function of NTnC-apo. It will be shown that the side-chain methyl group dynamics play an important role in the energetics of the calcium-induced structural change. Finally, the backbone order parameters of binding loop residues are used to calculate conformational entropy, and a quantitative contribution of entropy to binding affinity is obtained.

Consistency between the 500 and 600 MHz data

We chose to analyze the 500 and 600 MHz data separately, in order to obtain two independent characterizations of the dynamic properties of NTnC-apo. First, the experimental relaxation data are consistent between the two data sets. Using

$\tau_m = 4.86$ ns, $S^2 = 0.85$ and $\tau_e = 0$ ps in equation (1), one predicts a T_1^{600}/T_1^{500} ratio of 1.22 and a T_2^{600}/T_2^{500} ratio of 0.97. The observed 600/500 ratios agree well with the theoretical ones, with average values of 1.23 (±0.03) and 0.98 (±0.04) for T_1^{600}/T_1^{500} and T_2^{600}/T_2^{500}, respectively. The T_1^{600}/T_1^{500} ratio should agree well with the theory, except in special cases such as apo-calmodulin where large amplitude motions on a nanosecond time scale significantly shorten the observed T_1s. The agreement between the measured and theoretical T_1^{600}/T_1^{500} ratio is an indication of the absence of such motions in NTnC-apo.

As previously noted, the NOE^{600}/NOE^{500} ratio is larger than expected with an average of 1.11 (±0.06), and a theoretical ratio of 1.05 to 1.02 for τ_e in the 0 to 100 ps range. This larger than expected ratio is most likely due to experimental error. Closer inspection of the data indicates that the NOE^{600} is larger than expected. Using $\tau_m = 4.86$ ns and $\tau_e = 0$ ps, one predicts the maximum NOE^{500} and NOE^{600} to be 0.751 and 0.788, respectively. The 500 MHz data do not contain any NOE larger than the maximum value; Val45 has the largest NOE at 0.748 (±0.030). The 600 MHz data contain nine residues with $NOE^{600} > NOE_{max}$, ranging from 0.790 (±0.010) to 0.818 (±0.011). Of these nine residues, three have NOEs larger than the maximum value within experimental error, i.e. $(NOE^{600} - \sigma_{NOE}) > NOE_{max}$. The error present in the 600 MHz data will be corrected in future studies but was not in the data presented here. We believe the discrepancy is most likely due to water saturation. The systematic error present in the NOE data has been used herein to determine its effect on the analysis of the dynamics.

The overall correlation time, order parameters, and the anisotropic analysis are all consistent between the two fields. This not only supports a high level of confidence in the determined values, but also clearly indicates which relaxation parameters are critical to the analysis. Despite the error present in one of the NOE data sets, both analyses gave the same results, with the exception of the τ_e values. This observation is reassuring, since NOE values are usually the most imprecise relaxation measurements and, at least in the present study, the most inaccurate ones. We conclude that, unless one wishes to obtain accurate τ_e values, the precision and accuracy of the experimental NOE data are not critical to the analysis.

Although both data could have been fit together, and the goodness of the fit used to evaluate the confidence level on the determined parameters, treating the data separately has several advantages. First, consistency between two data sets is more easily appreciated than, for example, a low χ^2. Second, fitting of the data on some computers is significantly faster, since doubling the number of parameters in a fitting procedure more than doubles the necessary computing time, whether a minimization or a grid search is performed. We believe that obtaining relaxation parameters at two or more different field strengths and treating them independently is an excellent approach to validate the results obtained from the analysis. Other studies published recently have also used a similar approach (Phan *et al*., 1996; Tjandra *et al*., 1996).

Rotational correlation time and rotational diffusion anisotropy

We have determined the overall correlation time (τ_m) of NTnC-apo to be 4.86 (±0.15) ns at 29.6°C, under sample conditions listed in Materials and Methods. This value was obtained using the model-free analysis with the spectral density defined as a function of τ_m, S^2 and τ_e (equation (1)), and the assumption that the rotational motion is isotropic. With the assumption of isotropic motion, 16 residues required the inclusion of a conformational exchange term (R_{ex}) in the T_2 expression. In particular, the entire helix-A required R_{ex} terms in order to obtain a good fit. Although it is possible for an entire helix to undergo conformational exchange, it is not likely in the present case. If conformational exchange did occur in helix-A, one would expect to observe conformational exchange for residues in helix-B and helix-D which are packed on helix-A, especially since three Phe residues are located in helix-A. This was not observed.

Analysis of the relaxation parameters while considering rotational anisotropy indicated a significantly better fit for an axially symmetric diffusion tensor with $\tau_{m,eff}$, $D_\parallel/D_\perp$, θ and ϕ equal to 4.82 ns, 1.10, 8° and −118°, respectively. Anisotropic motion is a more plausible explanation for the relaxation parameters observed in helix-A than conformational exchange. The $\tau_{m,eff}$ determined while accounting for motional anisotropy is identical to the τ_m determined with the assumption of isotropic motion. This therefore justifies the assumption of isotropic motion for determination of the overall correlation time. The anisotropic diffusion of NTnC-apo is very small with $D_\parallel/D_\perp = 1.10$ and is consistent with the inertia tensor (1.00:0.91:0.85) calculated from the structure coordinates. Tjandra *et al*. (1995) showed that slight anisotropy ($D_\parallel/D_\perp = 1.17$) could be reflected in the observed relaxation parameters of ubiquitin. The present study shows that even smaller anisotropy can affect relaxation parameters.

As pointed out by Tjandra *et al*. (1995), motional anisotropy should be considered, especially if incorporation and interpretation of conformational exchange is attempted in the analysis. Although the molecule studied here is nearly spherical, slight motional anisotropy affects the observed relaxation parameters and anisotropy has to be considered. As suggested by recent studies (Lee *et al*., 1997; Luginbühl *et al*., 1997; Phan *et al*., 1996; Tjandra *et al*., 1995, 1996), motional anisotropy should always be carefully considered in the analysis of ^{15}N relaxation data.

Comparison with structural data

This study is the first to report experimental data on the backbone dynamics of TnC. Although the crystallographic *B*-factors and NMR rmsd reported with the X-ray and NMR structures are not direct measures of dynamics, a qualitative comparison of these values with the order parameters can be made. The per residue rmsd obtained from a family of NMR structures has no direct relation with the determined S^2; it is simply a reflection of the restraints used to generate the structures. Although per residue rmsd should not be interpreted in terms of flexibility, regions with small S^2 values should usually correspond to a higher rmsd in the ensemble of calculated structures. Comparison of the S^2 values determined here with the per residue backbone rmsd from the NMR structures of NTnC-apo (Gagné *et al.*, 1995) is illustrated in Figure 9. This comparison indicates that the lack of definition in the NMR structure for the N and C-terminal residues and in both calcium binding loops is largely due to flexibility. The correlation is however not perfect on a per residue basis in the calcium binding loops. This could be due to an ''over-constraining'' of the first residues in the loops, or a small lack of restraints for some later residues. Overall, the correlation between the backbone rmsd of the NMR structure and the S^2 is good, and there is no indication of a lack of restraints in the NMR structure. There is however a possibility of over-constraining around helix-N which was well-defined in the NMR structure from residue 7 and on. Despite the fact that several residues from helix-N could not be characterized here, all of the determined ones have an S^2 lower than the rest of the helices. Additionally, the S^2_{axis} of the Ala8 methyl group is lower than for most alanine residues (Figure 8(c)).

The value of the crystallographic *B*-factor is affected by several factors, but since internal motion is one of its major contributors, tendencies in the order parameter are usually, but not always, reflected in the value of the *B*-factor. Previous reports have shown that there is no quantitative correlation between *B*-factors and order parameters, but that a qualitative correlation usually exists (Mandel *et al.*, 1995; Powers *et al.*, 1993). A qualitative comparison of S^2 values from this study and *B*-factors from the crystal structure (Herzberg & James, 1988) is shown in Figure 9. The flexible regions of NTnC, as determined by the S^2 values, have large *B*-factors in the crystal structure. Interestingly, the disorder in helix-N, as suggested by the relaxation data, is in agreement with the X-ray data where helix-N residues have unusually large *B*-factors compared to the other helices. This terminal helix is packed on only one other helix, helix-D, and is therefore likely less stable than the other helices. Because of its location in space, helix-N could be partially unfolded without affecting the environment of the functional regions of NTnC, such as the calcium binding loop and the hydrophobic pocket.

Inspection of the order parameters of the methyl groups in relation to the calcium-induced structural change reveals some interesting features. As

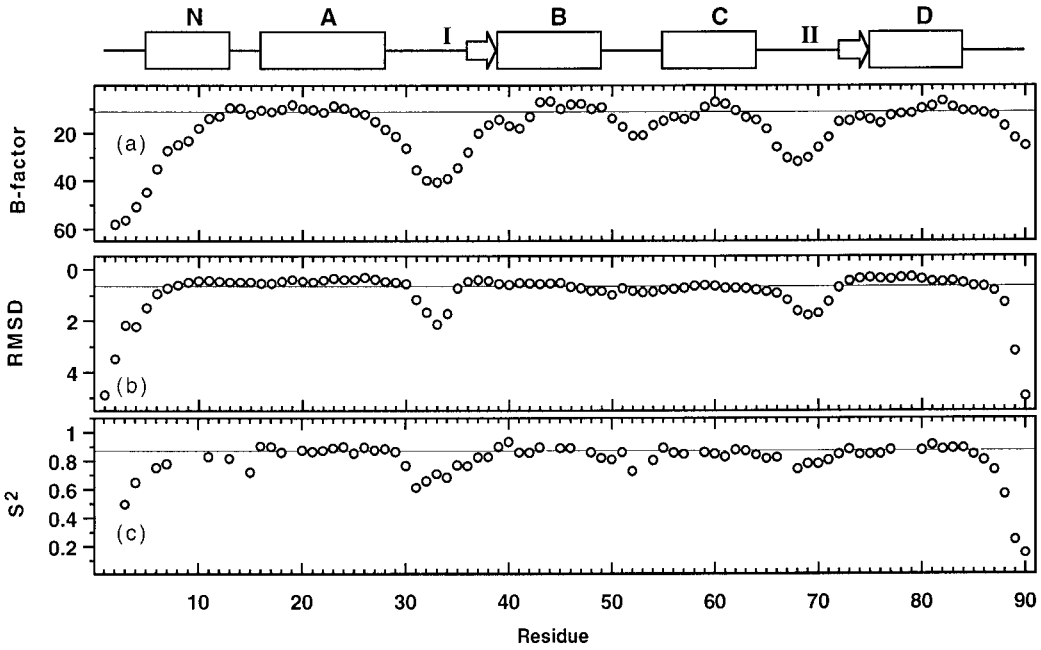

Figure 9. Comparison between the nitrogen *B*-factor (a) of the X-ray structure (Herzberg & James, 1988), the backbone RMSD (b) of the NMR structure (Gagné *et al.*, 1995) and the backbone order parameter (c) of the present study. The line in each plot represents the average value for helical residues. The secondary structure elements are shown on top as in Figure 4.

noted above, Met82 has an unusually high order parameter. Met82 is also the methionine residue which gets the most exposed upon calcium binding: an ASA increase of 63 Å^2 based on the NMR structures, and 51 Å^2 based on the X-ray structures. Note that the larger calcium-induced exposure of Met82 relative to other methionine residues is due to the open form (calcium saturated) and not to the apo structure, since all three buried methionine residues have essentially the same ASA in the apo structure. Since exposing hydrophobic residues is energetically expensive, one could think that the larger exposure of Met82 would contribute more to the cost of opening the structure. When the dynamics are taken into account, one sees a different picture. Assuming that the order parameter of Met82 will be more normal in the open form, i.e. around 0.2 (Figure 8(c)), this would correspond to a large gain in conformational entropy. Therefore the overall cost of exposing Met82 will be significantly smaller than the exposure of the other methionine residues, since those will not gain as much entropy upon the calcium-induced structural change.

In both the NMR and the crystal structures of NTnC-apo, the side-chain of Leu49 is more exposed than all other leucine side-chains by 20 to 30 Å^2. Despite this, Leu49 is less flexible than other leucine residues, as shown by its large order parameter (Figure 8(c)). When looking at the calcium-saturated structures, one finds that Leu49 is the only leucine side-chain that is exposed upon the structural change (73 Å^2 for the NMR structures, and 94 Å^2 for the X-ray structures). Again, a residue which gets significantly exposed is rigid in the apo form, and the energetic cost associated with exposing a hydrophobic side-chain can be reduced by a gain in conformational entropy. It is therefore clear that the dynamics of the methyl groups play a role in the energetics of calcium binding, and ultimately in the energetics of the calcium-induced structural change. Since the dynamics of the calcium saturated form have not been determined yet, we cannot provide a quantitative description of these energetics. It is however evident that future studies of methyl dynamics of calcium saturated NTnC would provide valuable understanding of the fine tuning which occurs in order for this protein to adequately perform its function.

Correlation between flexibility and calcium-binding affinity

The order parameters which were determined for the backbone amides of NTnC-apo show a value of ~0.85 for secondary structural elements, and lower values for loops and terminal regions, as is typical for many proteins. Although these measurements can be used to validate the apparent flexibility in the calculated NMR structure, interpretations of the backbone order parameters are often limited. Following earlier work of Akke *et al*. (1993), Yang & Kay (1996) recently presented an approach where contributions to conformational entropy arising from bond vector fluctuations measured from NMR-derived order parameters could be evaluated. We have used this approach to correlate flexibility and calcium-binding affinity.

There is a conformational entropic change associated with the binding of calcium to the sites of NTnC. This entropic change is defined as: $\Delta S_p = S_p^{Ca} - S_p^{apo}$, where S_p^{Ca} is the conformational entropy of the calcium-bound state and S_p^{apo} is the conformational entropy of the calcium-free state. Note that ΔS_p is the conformational entropy change of the protein only, and does not include any entropic contribution from solvent or calcium ions. One would therefore expect ΔS_p to be negative; this notion is supported by the calcium-saturated crystal structure data where the *B*-factors of the calcium binding loops are among the lowest (Figure 10(a)). The difference in calcium-induced ΔS_p between site I and site II is:

$$\Delta\Delta S_p = (S_p^{I,Ca} - S_p^{I,apo}) - (S_p^{II,Ca} - S_p^{II,apo}).$$

Ideally, dynamic data for both the apo and the calcium-saturated forms would be used to estimate $\Delta\Delta S_p$. Although relaxation data are readily available for the apo form, it is not possible to obtain the relevant NMR relaxation data for the calcium form. As pointed out previously (Gagné *et al*., 1995; Slupsky *et al*., 1995) NTnC dimerises upon calcium binding with a K_d of 0.8 mM (S. M. Gagné, unpublished data). Due to the value of K_d, the concentration required to obtain relaxation data for a 95% monomeric sample is too low (~20 μM) for NMR relaxation experiments. It is possible to make a sample which is predominantly dimeric; however, the dimeric state has no physiological relevance, and the dynamic properties of the dimer would likely be different from the monomer; thus, relaxation data for the dimer are not acceptable for the present study. One could take the monomer/dimer equilibrium into account in the analysis, but the larger number of variables that would be involved (one set for each state) would exceed the number of experimental parameters. Although relaxation data for the calcium form cannot be used quantitatively, we can extract qualitative information from it. Figure 10(b) shows the ^{15}N-T_2 relaxation data for the calcium-saturated form of NTnC at a concentration of 1.5 mM where NTnC is approximately 40% monomeric. As mentioned previously (Gagné *et al*., 1995), the spectral quality of NTnC-2Ca is significantly inferior to that of NTnC-apo because of broadening and overlap, and therefore only 24 residues can be characterized with confidence. The average T_2 of the calcium form is smaller due to increased molecular weight of the partial dimer. However, when compared with the T_2s in the calcium form, the relaxation data indicate that the calcium binding sites have lost their flexibility upon calcium binding; this is best illustrated by residues 32 to 34. That the calcium binding loops lose their flexibility similarly

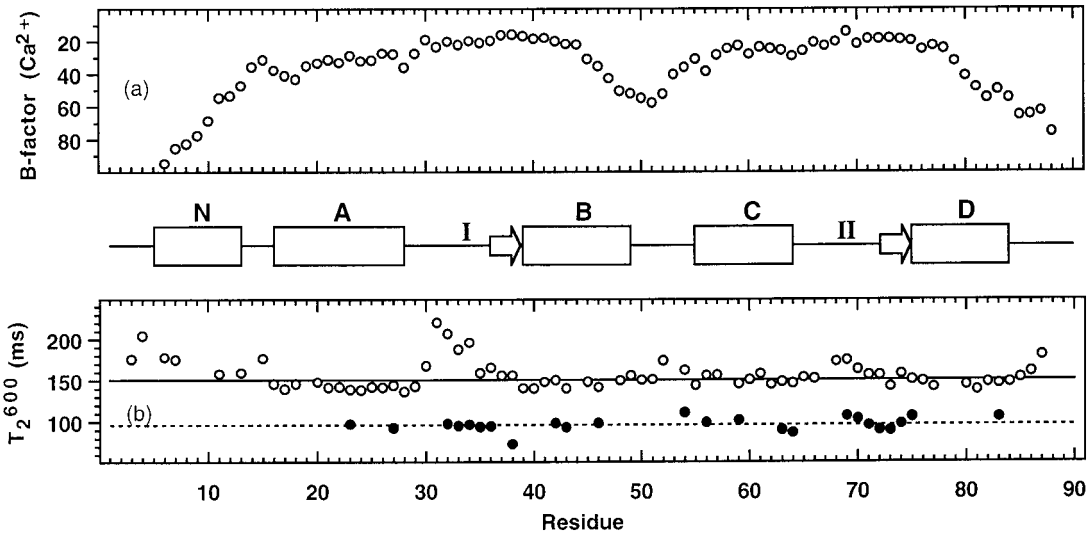

Figure 10. Crystallographic (a) and NMR (b) data showing the lack of flexibility in the calcium binding loops when calcium is bound. (a) The crystallographic *B*-factors are from the X-ray structure of NTnC-2Ca (Strynadka *et al.*, 1997). (b) The ^{15}N-T_2 of NTnC-2Ca at 600 MHz (●) are compared with the ^{15}N-T_2 of NTnC-apo (○) at the same field strength. The apo data are the same as shown in Figure 4(a). The calcium data were acquired on a 1.5 mM sample under the same conditions as for the apo data. The smaller number of characterized residues for NTnC-2Ca is due to overlap and to the poor spectral quality of the partially dimerized protein.

upon calcium binding is further supported by the X-ray *B*-factors of NTnC-2Ca (Figure 10(a)).

Although detailed information about the dynamics of the calcium form is not readily available, the partial information shown in Figure 10 allows us to determine that $S_p^{I,Ca} \approx S_p^{II,Ca}$. The difference, $\Delta\Delta S_p$, between site I and II is then reduced to: $\Delta\Delta S_p = S_p^{II,apo} - S_p^{I,apo}$. As proposed by Yang & Kay (1996), we can approximate the contribution to the difference in conformational entropy arising from differences in ps-ns timescale bond vector fluctuations, by using the following relation:

$$\Delta\Delta S_p = k \sum_n \ln \{[3 - (1 + 8S_{LZ,II})^{1/2}]/ [3 - (1 + 8S_{LZ,I})^{1/2}]\} \quad (14)$$

where k is Boltzmann's constant, $S_{LZ,I}$ and $S_{LZ,II}$ are order parameters determined by NMR for sites I and II, respectively, and $\Delta\Delta S_p$ is the difference in conformational entropic loss associated with calcium binding to site II and calcium binding to site I.

The difference in flexibility between sites I and II is highlighted in Figure 11. Residues in site I are substantially more disordered than residues in site II, with the exception of Thr39 and Lys40, which are more ordered than their homologous residues. This difference in order parameters can be translated into entropic difference using equation (14), and results of this calculation are shown in Table 4. The total difference in conformational entropy ($\Delta\Delta S_p$) between sites I and II in the apo state is 3.23 (±0.06) cal mol^{-1} K^{-1}. At the temperature here, this means that in the apo state site I is 0.98 (±0.02) kcal mol^{-1} more stable than site II in terms of conformational entropic free energy. As noted above, this difference is also an approximation of the difference in conformational entropic loss due to calcium binding. It has been shown previously that the two sites have different calcium binding affinities (Li *et al.*, 1995), and that the higher affinity is associated with site II (Gagné *et al.*, 1997).

Clearly, other entropic contributions from the solvent and calcium contribute significantly to the free energy of binding. Strynadka *et al.* (1997) have indicated that the structural nature of the calcium coordination in site I is a possible explanation for a weaker calcium affinity. Based on the NMR structure, they also proposed that conformational flexibility in site I may create an energetic cost in ordering this site for optimal calcium binding (Strynadka *et al.*, 1997). Based on the experimental data presented here, we show the larger conformational entropic cost associated with calcium

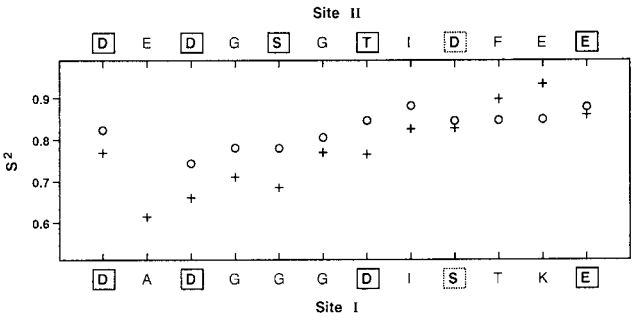

Figure 11. Comparison of the backbone order parameters between calcium binding site I (+) and II (○). The average of the 500 and 600 MHz determination is used. The sequences of site I and II are shown below and above the graph, respectively.

Table 4. Conformational entropy difference between site I and site II

Residue (site I–site II)	S^2 Site I[a]	S^2 Site II[a]	ΔS_P[b] (cal mol^{-1} K^{-1})	$-T\Delta S_P$[c] kcal mol^{-1})
30–66	0.768 ± 0.006	0.824 ± 0.007	−0.60	+0.18
31–67	0.614 ± 0.005	0.684 ± 0.008[d]	−0.47	+0.14
32–68	0.660 ± 0.006	0.744 ± 0.006	−0.64	+0.20
33–69	0.710 ± 0.006	0.780 ± 0.007	−0.61	+0.19
34–70	0.685 ± 0.005	0.780 ± 0.007	−0.80	+0.24
35–71	0.770 ± 0.006	0.805 ± 0.008	−0.36	+0.11
36–72	0.765 ± 0.006	0.846 ± 0.006	−0.91	+0.28
37–73	0.825 ± 0.006	0.881 ± 0.006	−0.81	+0.25
38–74	0.827 ± 0.006	0.845 ± 0.008	−0.23	+0.07
39–75	0.897 ± 0.007	0.847 ± 0.006	+0.83	−0.25
40–76	0.933 ± 0.007	0.849 ± 0.007	+1.68	−0.51
41–77	0.859 ± 0.006	0.878 ± 0.007	−0.30	+0.09
Sum			−3.23	+0.98 ± 0.02

[a] Average of the S^2 determined at 500 and 600 MHz. Errors are estimated from Monte Carlo analyses.
[b] Calculated using equation (14).
[c] Using a temperature of 302.75 K (29.6°C). Error estimated from Monte Carlo analyses.
[d] Relaxation parameters for residue 67 were not determined due to overlap in the HSQC spectra. Value extrapolated from neighboring residues (66 and 68) to reflect the tendency of homologous residue 31 relative to its own neighboring residues (30 and 32).

binding to site I to be approximately 1 kcal mol^{-1} at 30°C. It should be noted that this value is related to ps-ns timescale motions only, and that contributions from slower motions are not accounted for. However, the value of 1 kcal mol^{-1} is consistent with the dissociation constants previously measured (Li *et al*., 1995) for sites I and II of 16 μM and 1.7 μM, respectively. Therefore, conformational entropy is a major factor for the fine tuning of the calcium affinity in NTnC, and likely in other similar calcium binding proteins.

Concluding Remarks

The dynamic characteristics of TnC show two different levels of fine tuning of the calcium affinity. First, the affinity is directly adjusted by the amount of flexibility present in the calcium binding loops of the apo form. The difference in flexibility between site I and site II in the apo state results in a difference of 1 kcal mol^{-1} of conformational entropy; this is a major contribution to the difference in calcium affinity between the two sites. Since the binding of calcium triggers a large conformational change, a second and indirect level of fine tuning occurs in the apo state through the degree of flexibility of hydrophobic residues which are exposed upon calcium binding. Our results show that in TnC it is not necessarily the sidechains which are more buried in the apo state which have reduced motion, but often the ones which will be exposed upon calcium binding. It is clear from this work that a complete determination of the dynamic characteristics is necessary in order to fully understand how TnC and other proteins are fine tuned to appropriately carry out their function.

Materials and Methods

Sample preparation

Cloning, expression, and labeling of chicken [U-^{15}N]NTnC is as previously described (Gagné *et al*., 1994). [U-^{13}C; U-^{15}N; U-40% ^{2}H]NTnC was obtained in a similar manner, except that expression was performed in a 50% ^2H_2O aqueous medium. The level of deuteration was determined from mass spectrometry, assuming a minimum level of 95% for ^{15}N and ^{13}C. To obtain metal-free NTnC, 14 mg of protein was dissolved in 0.5 ml of 100 mM EDTA, applied to a 1.5 cm × 90 cm G-25 gel filtration column equilibrated and eluted with 25 mM NH_4HCO_3, and monitored at $\lambda = 254$ nm. The pooled fractions were lyophilized, twice redissolved in water, and lyophilized again to ensure removal of NH_4HCO_3. Milli-Q deionized water was used in all steps. The NMR sample was prepared by dissolving 10 mg of metal-free NTnC in 0.5 ml of 100 mM KCl in 90% H_2O/10% ^2H_2O. To the sample was added 5 μl of 100 mM DSS and 5 μl of 1.3% (w/v) NaN_3. EDTA was also added to a concentration of 10 mM to ensure that the sample was completely in the apo form. The pH was adjusted to 6.7 with HCl and or NaOH prior to transfer to the NMR tube.

Data acquisition: ^{15}N relaxation experiments

^{15}N relaxation experiments were performed at a temperature of 29.6°C on Varian UNITY Inova 500 and Varian UNITY 600 spectrometers both equipped with *z*-axis pulsed field gradient, triple resonance probes. The ^{15}N-T_1, ^{15}N-T_2 and ^{15}N-{^{1}H}-NOE experiments were performed using the pulse sequences from Farrow *et al*. (1994).

The T_1^{500}, T_2^{500} and T_2^{600} were acquired once, using ^{15}N relaxation delays of [11, 33, 100, 178, 255, 355, 477, 633, 833, and 1143 ms], [17, 33, 50, 66, 83, 99, 116, 132, 149, 165, and 182 ms], and [16, 33, 49, 65, 81, 98, 114, 130, 146, 163, and 179 ms], respectively. The T_1^{600} was acquired twice, using ^{15}N relaxation delays of [33, 100, 178, 255, 355, 477, 633, 833, and 1143 ms] and [11, 33, 100, 178, 255, 355, 477, 633, 833, and 1143 ms]. Field strengths of 6.5, 3.8, 5.3 and 4.3 kHz were used for the

^{15}N hard pulses in the T_1^{500}, T_2^{500}, T_1^{600}, and T_2^{600} experiments, respectively. WALTZ-16 decoupling (Shaka *et al.*, 1983) of ^{15}N during acquisition was performed using field strengths of 1.2 and 0.8 kHz for the 500 and 600 MHz data, respectively. The relaxation delay between transients was three seconds for the T_2^{500} and T_2^{600} experiments, and one second for the T_1^{500} experiment. The two T_1^{600} data sets were acquired using different relaxation delays of one and 1.5 seconds. The number of transients per complex $t1$ point was 8 or 16.

^{15}N-{^{1}H} steady-state NOEs were obtained by acquiring spectra with and without ^{1}H saturation applied before the start of the experiment. ^{1}H saturation was achieved with the use of 120° ^{1}H pulses applied every 5 ms (Markley *et al.*, 1971). A saturation time of three seconds was used in all NOE experiments. The NOE^{500} experiment was repeated three times, with slightly different parameters. The first NOE^{500} data set used a field of 6.5 kHz for ^{15}N hard pulses, 1.1 kHz for WALTZ-16 decoupling, and 10.6 kHz for ^{1}H saturation. The other two data sets used a field of 5.1 kHz for hard pulses, 1.0 kHz for WALTZ-16 decoupling, and 10.7 kHz for ^{1}H saturation. The first and third data sets were obtained with 64 transients per complex $t1$ point, and relaxation delays of one and four seconds for the spectra with and without saturation. The second data set used 48 transients per complex $t1$ point and relaxation delays of two and five seconds for the spectra with and without saturation. The NOE^{600} experiment was repeated four times. All four data sets were obtained with a field of 5.3 kHz for ^{15}N hard pulses and 0.8 kHz for WALTZ-16 decoupling, and with 64 transients per complex $t1$ point. The first NOE^{600} data set used relaxation delays of one and four seconds for the experiment with and without saturation, respectively, whereas the other three data sets used two and five seconds for the same corresponding delays. ^{1}H saturation was accomplished with a field of 10.4 kHz for the first NOE^{600} data set, and a field of 10.7 kHz for the other three data sets.

The spectral widths used for all 500 MHz experiments were 7000 and 1300 Hz for ^{1}H and ^{15}N, respectively. The corresponding spectral widths for the 600 MHz experiments were 8000 and 1560 Hz. The acquisition times in $t1$ (^{15}N) and $t2$ (^{1}H) were 74 and 73 ms, respectively, for all experiments. Other various delays and gradient strengths were as described by Farrow *et al.* (1994).

Data acquisition: ^{2}H relaxation experiments

The ^{2}H relaxation experiments were performed at 30.9°C on a Varian UNITY + 600 spectrometer equipped with z-axis pulsed field gradient and triple resonance probe. The ^{2}H-T_1 and ^{2}H-$T_{1\rho}$ were obtained using the approach described by Muhandiram *et al.* (1995) with the [U-^{13}C; U-^{15}N; U-40% ^{2}H]-NTnC sample.

Measurement of $T_1^{I_zC_zD_z}$, $T_1^{I_zC_zD_y}$ and $T_1^{I_zC_z}$ were made once with relaxation delays of [0.05, 7, 14, 23, 27, 32, 44, 56, 77, and 90 ms], [0.25, 1.3, 2.8, 4.4, 6.2, 8.4, 10.9, 15.1, 20, and 28 ms], and [0.05, 7, 14, 23, 27, 32, 44, 56, 71, and 90 ms], respectively. The spectral widths were 9000.9 and 5494.5 Hz for ^{1}H and ^{13}C, respectively. All data sets were recorded as 152 × 576 complex matrices, with 32 transients per $t1$ increment for the $T_1^{I_zC_zD_z}$ and $T_1^{I_zC_zD_y}$ experiments, and 16 transients per $t1$ increment for the $T_1^{I_zC_z}$ experiment. The relaxation delay between transients was 1.7 seconds for all experiments. Field strengths, gradients and delays were as described by Muhandiram *et al.* (1995).

Data processing

All spectra were processed using the NMRPipe software (Delaglio *et al.*, 1995). The *ranceY.M* macro from the NMRPipe package was used to generate pure absorptive 2D line shapes from the sensitivity-enhanced data (^{15}N experiments only). Although not mandatory, removal of the residual water signal was performed through the use of time domain polynomial subtraction (NMRPipe function *POLY-time*). ^{1}H-^{15}N spectra were processed using a 90° shifted sine apodization function in $F2$ (^{1}H) and a 90° shifted sine-squared function in $F1$ (^{15}N). ^{1}H-^{13}C spectra were processed using a 60° shifted sine-squared apodization function in both dimensions. The time-domain data in $t1$ was extended through complex linear prediction by 32 and 45 complex points for the 500 and 600 ^{1}H-^{15}N spectra, respectively, and by 104 points for the ^{1}H-^{13}C spectra. Both dimensions were baseline corrected using the *POLY-auto* function in NMRPipe.

The first 2D spectra of the ^{15}N-T_1^{500} experiment was manually peak-picked using PIPP (Garrett *et al.*, 1991), and all other ^{1}H–^{15}N 2Ds were automatically peak-picked using the STAPP program (Garrett *et al.*, 1991). Peak-picking of the ^{1}H-^{13}C 2Ds was also automated in a similar way. Peak intensities were used in all cases. T_1, T_2 and $T_{1\rho}$ decay curves were fitted to a two-parameter function of the form:

$$I(t) = I_0 \exp(-t/T_{1,2,1\rho}) \tag{15}$$

where $I(t)$ is the intensity after a delay time t and I_0 is the intensity at time $t = 0$. Fitting was accomplished with the xcrvfit program (executable available at the following address: http://www.pence.ualberta.ca). The uncertainty in the T_1 and T_2 values were approximated from the non-linear least-squares fit. Uncertainties obtained using this approach were found to be slightly larger than those obtained from a Monte Carlo simulation. Steady-state NOE values were obtained from the ratio of the intensities of experiments recorded with and without proton saturation. The uncertainty in the NOE value was approximated from the baseline noise levels as described previously (Farrow *et al.*, 1994).

Acknowledgments

This research is supported by the Medical Research Council of Canada and the Protein Engineering Network Center of Excellence (PENCE). We thank M. X. Li and L. B. Smillie for assistance with sample preparation; G. McQuaid for keeping the spectrometer at optimum performance; Mission Control (J. L. Willard, T. Jellard and R. Boyko) for computer expertise; and J. D. Forman-Kay for providing the 600 MHz NMR spectrometer which was used in the ^{2}H relaxation experiments.

References

Abragam, A. (1961). *Principles of Nuclear Magnetism*, Clarendon Press, Oxford.

Akke, M., Brüschweiler, R. & Palmer, A. G. (1993). NMR order parameters and free energy: an analytical approach and its application to cooperative Ca^{2+} binding by calbindin D_{9k}. *J. Am. Chem. Soc.* **115**, 9832–9833.

Bevington, P. R. & Robinson, D. K. (1992). *Data Reduction and Error Analysis for the Physical Sciences,* 2nd edit., McGraw-Hill, New York.

Carson, M. (1987). Ribbon models of macromolecules. *J. Mol. Graphics,* **5**, 103–106.

Clore, G. M., Driscoll, P. C., Wingfield, P. T. & Gronenborn, A. M. (1990a). Analysis of the backbone dynamics of interleukin-1 beta using two-dimensional inverse detected heteronuclear ^{15}N-^{1}H NMR spectroscopy. *Biochemistry,* **29**, 7387–7401.

Clore, G. M., Szabo, A., Bax, A., Kay, L. E., Driscoll, P. C. & Gronenborn, A. M. (1990b). Deviations from the simple two-parameter model-free approach to the interpretation of nitrogen-15 nuclear magnetic relaxation of proteins. *J. Am. Chem. Soc.* **112**, 4989–4991.

Delaglio, F., Grzesiek, S., Vuister, G. W., Zhu, G., Pfeifer, J. & Bax, A. (1995). NMRPipe: a multidimensional spectral processing system based on UNIX pipes. *J. Biomol. NMR,* **6**, 277–293.

Farah, C. S. & Reinach, F. C. (1995). The troponin complex and regulation of muscle contraction. *FASEB J.* **9**, 755–767.

Farrow, N. A., Muhandiram, R., Singer, A. U., Pascal, S. M., Kay, C. M., Gish, G., Shoelson, S. E., Pawson, T., Forman-Kay, J. D. & Kay, L. E. (1994). Backbone dynamics of a free and a phosphopeptide-complexed Src homology 2 domain studied by ^{15}N NMR relaxation. *Biochemistry,* **33**, 5984–6003.

Findlay, W. A., Sönnichsen, F. D. & Sykes, B. D. (1994). Solution structure of the TR1C fragment of skeletal muscle troponin-C. *J. Biol. Chem.* **269**, 6773–6778.

Gagné, S. M., Tsuda, S., Li, M. X., Smillie, L. B. & Sykes, B. D. (1995). Structures of the troponin C regulatory domains in the apo and calcium-saturated states. *Nature Struct. Biol.* **2**, 784–789.

Gagné, S. M., Tsuda, S., Li, M. X., Chandra, M., Smillie, L. B. & Sykes, B. D. (1994). Qualification of the calcium-induced secondary structural changes in the regulatory domain of troponin-C. *Protein Sci.* **3**, 1961–1974.

Gagné, S. M., Li, M. X. & Sykes, B. D. (1997). Mechanism of direct coupling between binding and induced structural change in regulatory calcium binding proteins. *Biochemistry,* **36** (15), 4386–4392.

Garrett, D. S., Powers, R., Gronenborn, A. M. & Clore, G. M. (1991). A common sense approach to peak picking in two-, three-, and four-dimensional spectra using automatic computer analysis of contour diagrams. *J. Magn. Reson.* **95**, 214–220.

Herzberg, O. & James, M. N. G. (1988). Refined crystal structure of troponin C from turkey skeletal muscle at 2.0 Å resolution. *J. Mol. Biol.* **203**, 761–779.

Herzberg, O., Moult, J. & James, M. N. G. (1986). A model for the Ca^{2+}-induced conformational transition of troponin C. *J. Biol. Chem.* **261**, 2638–2644.

Kay, L. E., Forman-Kay, J. D., McCubbin, W. D. & Kay, C. M. (1991). Solution structure of a polypeptide dimer comprising the fourth Ca^{2+}-binding site of troponin C by nuclear magnetic resonance spectroscopy. *Biochemistry,* **30**, 4323–4333.

Kay, L. E., Muhandiram, D. R., Farrow, N. A., Aubin, Y. & Forman-Kay, J. D. (1996). Correlation between dynamics and high affinity binding in an SH2 domain interaction. *Biochemistry,* **35**, 361–368.

Leavis, P. C. & Gergely, J. (1984). Thin filament proteins and thin filament-linked regulation of vertebrate muscle contraction. *CRC Crit. Rev. Biochem.* **16**, 235–305.

Lee, L. K., Rance, M., Chazin, W. J. & Palmer, A. G., III (1997). Rotational diffusion anisotropy of proteins from simultaneous analysis of ^{15}N and ^{13}Cα nuclear spin relaxation. *J. Biomol. NMR,* **9**, 287–298.

Li, M. X., Gagné, S. M., Tsuda, S., Kay, C. M., Smillie, L. B. & Sykes, B. D. (1995). Calcium binding to the regulatory N-domain of skeletal muscle troponin C occurs in a stepwise manner. *Biochemistry,* **34**, 8330–8340.

Lipari, G. & Szabo, A. (1982a). Model-free approach to the interpretation of nuclear magnetic resonance relaxation in macromolecules. 1. Theory and range of validity. *J. Am. Chem. Soc.* **104**, 4546–4559.

Lipari, G. & Szabo, A. (1982b). Model-free approach to the interpretation of nuclear magnetic resonance relaxation in macromolecules. 2. Theory and range of validity. *J. Am. Chem. Soc.* **104**, 4559–4570.

Luginbühl, P., Pervushin, K. V., Iwai, H. & Wüthrich, K. (1997). Anisotropic molecular rotational diffusion in ^{15}N spin relaxation studies of protein mobility. *Biochemistry,* **36**, 7305–7312.

Mandel, A. M., Akke, M. & Palmer, A. G. (1995). Backbone dynamics of *Escherichia coli* ribonuclease HI: correlations with structure and function in an active enzyme. *J. Mol. Biol.* **246**, 144–163.

Markley, J. L., Horsley, W. J. & Klein, M. P. (1971). Spin-lattice relaxation measurements in slowly relaxing complex spectra. *J. Chem. Phys.* **55**, 3604–3605.

Muhandiram, D. R., Yamazaki, T., Sykes, B. D. & Kay, L. E. (1995). Measurements of ^{2}H T_1 and $T_{1\rho}$ relaxation times in uniformly ^{13}C-labeled and fractionally ^{2}H-labeled proteins in solution. *J. Am. Chem. Soc.* **117**, 11536–11544.

Ohtsuki, I., Maruyama, K. & Ebashi, S. (1986). Regulatory and cytoskeletal proteins of vertebrate skeletal muscle. *Advan. Protein Chem.* **38**, 1–67.

Phan, I. Q. H., Boyd, J. & Campbell, I. D. (1996). Dynamic studies of a fibronectin type I module pair at three frequencies: anisotropic modelling and direct determination of conformational exchange. *J. Biomol. NMR,* **8**, 369–378.

Powers, R., Clore, G. M., Garrett, D. S. & Gronenborn, A. M. (1993). Relationships between the precision of high-resolution protein NMR structures, solution-order parameters, and crystallographic B factors. *J. Magn. Reson. ser. B,* **101**, 325–327.

Satyshur, K. A., Rao, S. T., Pyzalska, D., Drendal, W., Greaser, M. & Sundralingham, M. (1988). Refined structure of chicken skeletal muscle troponin C in the two calcium state at 2 Å resolution. *J. Biol. Chem.* **263**, 1628–1647.

Shaka, A. J., Keeler, J., Frenkiel, T. & Freeman, R. (1983). An improved sequence for broadband decoupling: WALTZ-16. *J. Magn. Reson.* **52**, 335–338.

Shaw, G. S. & Sykes, B. D. (1996). NMR solution structure of a synthetic troponin C heterodimeric domain. *Biochemistry,* **35**, 7429–7438.

Shaw, G. S., Hodges, R. S. & Sykes, B. D. (1992). Determination of the solution structure of a synthetic two-site calcium-binding homodimeric protein domain by NMR spectroscopy. *Biochemistry,* **31**, 9572–9580.

Slupsky, C. M. & Sykes, B. D. (1995). NMR solution structure of calcium-saturated skeletal muscle troponin C. *Biochemistry,* **34**, 15953–15964.

Slupsky, C. M., Kay, C. M., Reinach, F. C., Smillie, L. B. & Sykes, B. D. (1995). Calcium-induced dimerization of troponin C: mode of interaction and use

of trifluoroethanol as a denaturant of quaternary structure. *Biochemistry*, **34**, 7365–7375.
Spyracopoulos, L., Gagné, S. M., Gronwald, W., Kay, L. E. & Sykes, B. D. (1998). NMR studies of protein sidechain dynamics: examples from antifreeze and calcium-regulatory proteins. In *Protein Dynamics, Function and Design* (Jardetzky, O. & Lefèvre, J.-F., eds), Plenum Press, New York and London, in the press.
Strynadka, N. C. J., Chernaia, M., Sielecki, A. R., Li, M. X., Smillie, L. B. & James, M. N. G. (1997). Structural details of a calcium-induced molecular switch: X-ray crystallographic analysis of the calcium-saturated N-terminal domain of troponin C at 1.75 Å resolution. *J. Mol. Biol.* **273**, 238–255.
Tjandra, N., Feller, S. E., Pastor, R. W. & Bax, A. (1995). Rotational diffusion anisotropy of human ubiquitin from ^{15}N NMR relaxation. *J. Am. Chem. Soc.* **117**, 12562–12566.
Tjandra, N., Wingfield, P., Stahl, S. & Bax, A. (1996). Anisotropic rotational diffusion of perdeuterated HIV protease from ^{15}N NMR relaxation measurements at two magnetic fields. *J. Biomol. NMR,* **8**, 273–284.
Wang, A. C. & Bax, A. (1993). Minimizing the effects of radio-frequency heating in multidimensional NMR experiments. *J. Biomol. NMR,* **3**, 715–720.
Wolfram, S. (1996). *The Mathematica Book,* 3rd edit., Wolfram Media/Cambridge University Press.
Yang, D. & Kay, L. E. (1996). Contributions to conformational entropy arising from bond vector fluctuations measured from NMR-derived order parameters: Application to protein folding. *J. Mol. Biol.* **263**, 369–382.
Zot, A. S. & Potter, J. D. (1987). Structural aspects of troponin-tropomyosin regulation of skeletal muscle contraction. *Annu. Rev. Biophys. Biophys. chem.* **16**, 535–559.

Edited by P. E. Wright

(Received 28 October 1997; received in revised form 10 February 1998; accepted 11 February 1998)

http://www.hbuk.co.uk/jmb

Supplementary material comprising three Tables is available from JMB Online.